Distributed Coordination of Islanded Microgrid Clusters Using a Two-layer Intermittent Communication Network

Lu, Xiaoqing; Lai, Jingang; Yu, Xinghuo; Wang, Yaonan; Guerrero, Josep M.

Published in:
IEEE Transactions on Industrial Informatics

DOI (link to publication from Publisher):
10.1109/TII.2017.2783334

Publication date:
2018

Document Version
Accepted author manuscript, peer reviewed version

Distributed Coordination of Islanded Microgrid Clusters Using a Two-layer Intermittent Communication Network

Xiaoqing Lu, Jingang Lai, Xinghuo Yu, *Fellow, IEEE*, Yaonan Wang, Josep M. Guerrero, *Fellow, IEEE*

***Abstract*—This paper proposes a distributed hierarchical cooperative (DHC) control strategy for a cluster of islanded microgrids (MGs) with intermittent communciation, which can regulate the frequency/voltage of all distributed generators (DGs) within each MG as well as ensure the active/reactive power sharing among MGs. A droop-based distributed secondary control (DSC) scheme and a distributed tertiary control (DTC) scheme are presented based on the iterative learning mechanics, by which the control inputs are merely updated at the end of each round of iteration, and thus each DG only needs to share information with its neighbors intermittently in a low-bandwidth communication manner. A two-layer sparse communication network is modeled by pinning one or some DGs (pinned DGs) from the lower network of each MG to constitute an upper network. Under this control framework, the tertiary level generates the frequency/voltage references based on the active/reactive power mismatch among MGs while the pinned DGs propagate these references to their neighbors in the secondary level, and the frequency/voltage nominal set-points for each DG in the primary level can be finally adjusted based on the frequency/voltage errors. Stability analysis of the two-layer control system is given, and sufficient conditions on the upper bound of the sampling period ratio of the tertiary layer to the secondary layer are also derived. The proposed controllers are distributed, and thus allow different numbers of heterogeneous DGs in each MG. The effectiveness of the proposed control methodology is verified by the simulation of an AC MG cluster in Simulink/SimPowerSystems.**

***Index Terms*—Distributed control, microgrid cluster, secondary control, communication network.**

Manuscript received July 16, 2017; revised October 20, 2017; accepted December 4, 2017. This work was supported in part by the National Natural Science Foundation of China under Grant 61773158, Grant 51707071, and Grant 61403133, in part by the Australia Research Council under Grant 140100544, in part by the National Postdoctoral Program for Innovative Talents of China under Grant BX201600055, in part by the Postdoctoral Foundation of China under Grant 2017M610475. Paper no. TII-17-2447. (Corresponding author: X. Lu.)

X.Q. Lu is with the School of Power and Mechanical Engineering, Wuhan University, Wuhan 430072, PR China and also with the School of Engineering, RMIT University, Melbourne VIC 3001, Australia (e-mail:henanluxiaoqing@163.com).

J.G. Lai is with the School of Electrical and Electronic Engineering, Huazhong University of Science and Technology, Wuhan 430074, PR China and also with the School of Engineering, RMIT University, Melbourne VIC 3001, Australia (e-mail:jinganglai@126.com).

X. Yu is with the School of Engineering, RMIT University, Melbourne, VIC 3001, Australia (e-mail:x.yu@rmit.edu.au).

Y. Wang is with the College of Electrical and Information Engineering, Hunan University, Changsha 410082, PR China (e-mail: yaonan@hnu.edu.cn).

J.M. Guerrero is with the Department of Energy Technology, Aalborg University, 9220 Aalborg, Denmark (e-mail:joz@et.aau.dk).

Color versions of one or more of the figures in this paper are available online at http://ieeexplore.ieee.org.

Digital Object Identifier XX.XXXX/TII.2017.XXXXXXX

I. Introduction

As an effective integration of DGs, loads, and storage units via DC/AC inverters [1], MGs can operate in both grid-connected and islanded modes. For enabling maximum utilization of renewable sources and also efficiently suppressing stress and aging of the components of MGs [2],[3], matching power transfer between MGs to form various MG clusters has become the future trend of the smart distribution grids.

Up to now, many literatures focus on the power quality issues (i.e., primary [4] and secondary control [5],[6]) within a MG in the islanded mode and the transient behaviors (i.e., tertiary control [7],[8]) that may occur when switching on and off from the utility grid [9]. The existing secondary control strategies include the feedback linearization voltage regulation method [10], a novel DSC approach that requires each local controller communicate with all the others across the MG [11], several compromise methods to solve the inherent contradiction between voltage regulation and reactive power sharing [12],[13],[14], and the frequency/voltage controller to robust against uncertain communication links [15], to name just a few. Tertiary control is used to realize the power flow balance among MGs and utility grid [16], including the optimization control method to achieve autonomous equal power sharing among DC-DC converters [17], and the voltage unbalance compensation scheme [8], and so on.

Although the above studies address many significant research challenges within MGs, to the best of our knowledge, there are only a few literatures focus on multiple MGs from the perspective of a smart microgrid network [9]. To this end, two important issues should be considered. One is the overlay topology design problem so as to maximize the usage of renewable DGs, and the other is the power flow and power quality problem among multiple MGs.

To address the first problem, a reliable overlay topology design method for the smart microgrid network was presented very early [9], then [18] studied a reliability and redundancy design of a smart grid wireless communications system in view of demand side management, afterwards an integrated reconfigurable control and self-organizing communication framework was established for community resilience microgrids [19]. More recently, a voltage-frequency management technique for remote islanded MGs was also proposed

[20], by which an overloaded MG or the one with excessive renewable generation can be coupled to one or more suitable neighboring islanded MGs at the lowest cost. Assuming the multiple MG network is previously designed, some control approaches for multiple AC or DC MG clusters have been proposed to solve the second problem. The existing results for DC MG clusters include a tertiary power flow scheme by adopting an droop-based centralized secondary control method [21], and a hierarchical control framework to avoid the centralized control mode [22], etc. Unlike DC MG clusters, the control issues of AC MG clusters involve the control of frequency and phase, reactive power, and power quality, thus still faces big challenges [21]. The only relevant results include a clustering and cooperative control strategy by organizing DGs into several clusters for grid-connected AC MGs [23], and a distributed power management scheme for intertied AC MGs based on the droop operating principles [24], etc. However, the adopted P/Q control mode in [23] is generally not suitable for multiple MG clusters in an islanded mode, while the power management scheme in [24] does not take into account the proportional power sharing accurately among MGs.

By analysis, to maximum utilize of renewable sources, the cyber topology structure of a MG cluster will finally present a hierarchical and clustering characteristic regardless of how the multiple MGs are dynamically coupled and recombined. In this situation, it is necessary to consider the time-scale separation requirements for the hierarchical interactive information flow that integrated in the cluster-oriented physical network when we try to address the power flow and power quality problem within each MG or among multiple MGs. Note that both secondary and tertiary levels (except primary level) generally allow information exchange among DGs within a MG via a centralized, decentralized, or distributed manner [8],[25],[26]. This inspires us to study the multiple AC MGs from the perspective of a special network that possess some cluster-oriented two-layer topology structure. In view of this, by establishing a two-layer communication network for a cluster of islanded AC MGs, this paper presents a DHC strategy, consisting of a DTC and a DSC schemes respectively corresponding to the upper and lower networks, that are equipped with an intermittent communication mechanics. The main contributions are listed below:

i) The consensus-based DTC scheme allows one or some DGs within each MG to be pinned to formulate the tertiary layer, and only the power flow mismatch information of the pinned DGs is needed to exchange in a distributed way, which is different from most of the centralized tertiary schemes [16],[27]. The pinning-based DSC scheme contains a voltage observer, under which the average voltage magnitude of all DGs within each MG can be regulated to the reference and then the accurate reactive power sharing among all MGs can be realized simultaneously. Thus, it extends the results of [13],[14],[15] to the case of voltage and reactive power management with intermittent communication.

ii) All the intermittent communication controllers are in the discrete form, with which each DG only needs to access partial or limited knowledge of the system parameters, perform merely local measurements, and then, communicate with its neighbors intermittently. It in turn greatly reduces the communication costs and makes our results essentially different from the existing continuous-time communication methods [10], [28]. Different from [11], [25], a sparse two-layer cyber network is sufficient to support the proposed scheme, even allowing only one DG from each MG to access the references. Besides the plug-and-play capacity of MG level, the proposed scheme also possesses high robustness against time delays, data drop-out, link failure, even for the interval uncertainties within information exchanges among all DGs or MGs.

iii) Different from the existing single-layer communication networks [16],[23],[24], the two-layer communication network are designed with different dynamics and time scales for each layer, which can more effectively meet the time-scale separation requirements for the hierarchical interactive information flow that integrated in the cluster-oriented physical network. Unlike many relevant hierarchical results that analyze the stability of each layer separately [8],[13],[15], this paper presents the detailed stability analysis on the whole two-layer dynamical system. Sufficient conditions, in terms of network connectivity and the sampling period ratio of the tertiary layer to the secondary layer, are finally derived, which will provide some inspiration for the future cluster-oriented two-layer network topology design of MG clusters.

The rest of this paper is organized as follows. The configuration of an AC MG cluster and the DHC strategy are presented in Sec. II and III, respectively. Sec. IV gives the detailed analysis of the system. After that, the numerical results are analyzed via an AC MG cluster system consisting of three AC MGs in Sec. V before one concludes the work in Sec. VI.

II. MG Cluster Configuration

To begin with, some necessary notations are listed. Let $\mathcal{I}_n = \{1, 2, \cdots, n\}$ and $\bar{\mathcal{I}}_n = \{0, 1, 2, \cdots, n\}$ be the finite index sets, $\bar{\mathcal{Z}} = \{0, 1, 2, \cdots\}$ be the set of nonnegative integers, $\lceil a \rceil$ be the maximum integer that does not exceed the scalar a, I_n be the $n \times n$ identity matrix, $1_n = (1, \cdots, 1)^T \in R^n$, and $\otimes$ be the Kronecher product. For any vectors $x = (x_1, \cdots, x_n)^T$ and $y = (y_1, \cdots, y_n)^T$, denote $x \odot y = (x_1 y_1, \cdots, x_n y_n)^T$. For any n-dimensional symmetric matrix A, let $\lambda_1(A) \leq \lambda_2(A) \leq \cdots \leq \lambda_n(A)$ be the n eigenvalues of A with an increasing sort.

A. The proposed DHC control framework

We will adopt the pinning control algorithm from the leader-follower-based multi-agent control theory [28],[29]. For MGs with large number of DGs, a pinning-based method is very suitable since it only needs a small fraction of DGs to be controlled by simple feedback controllers. Thus it is naturally used to reduce the number of DG controllers and further reduce the communication and control costs.

Consider a MG cluster containing M MGs labeled $\mathrm{MG}_1, \cdots, \mathrm{MG}_s, \cdots, \mathrm{MG}_M$, where MG_s consists of m_s DGs labeled $(s, 1)$ through (s, m_s). The DHC framework employs a sparse two-layer communication network to implement the information exchange and control in different control levels, as shown in Fig. 1. As seen, the lower communication network is responsible to the secondary frequeny/voltage control within

This article has been accepted for publication in a future issue of this journal, but has not been fully edited. Content may change prior to final publication. Citation information: DOI 10.1109/TII.2017.2783334, IEEE Transactions on Industrial Informatics

each MG, while the upper communication network enables to realize the tertiary active/reactive power control among MGs.

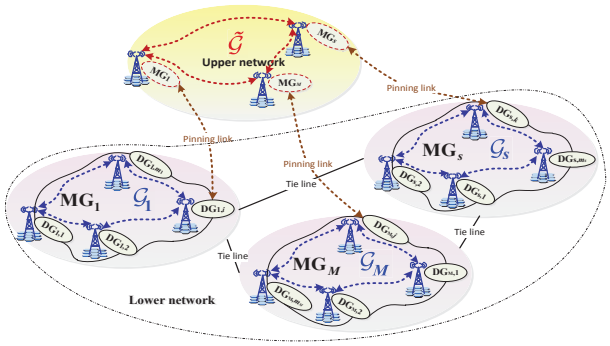

Fig. 1. A MG cluster supported by two-layer communication networks (the upper network located in the yellow region and the lower network located in the pink region), where the red and blue dotted lines represent the cyber links while the black solid lines represent the physical links.

We aim to address the time-scale matching problem in term of different sampling times, corresponding to each layer of the cluster-oriented two-layer communication network. In detail, for each MG_s, there is a secondary communication network (the pink region in Fig. 1), $\mathcal{G}_s$, corresponding to the information exchange among all DGs within MG_s. It is assumed that each $\mathrm{DG}_{s,i}$ within MG_s only needs to communicate with its neighboring DGs through the lower network, $\mathcal{G}_s$, and the reference information generated by the upper network are available to a small part or even only one following $\mathrm{DG}_{s,\mathrm{pin}}$ (as shown in Fig. 1). Herein, by pinning one or some DGs, $\mathrm{DG}_{s,\mathrm{pin}}$, from each MG_s, the tertiary communication network, $\tilde{\mathcal{G}}$, can be then formulated (the yellow region in Fig. 1). Note that all cyber networks are not necessary to own the same topology structures as the physical networks, thus not all DGs or MGs in large-scale systems need to be in a direct contact.

The proposed DHC strategy consists of the primary, secondary, and tertiary control levels. For the ith DG in the sth MG ($i \in \mathcal{I}_{m_s}$ and $s \in \mathcal{I}_M$), $\mathrm{DG}_{s,i}$, its power outputs are adjusted by the primary control through the power, voltage, and current control loops [15]. To compensate the voltage/frequency deviations caused by the primary stage, the secondary control is applied to generate the frequency/voltage nominal set-points, $\omega_{s,i}^{\mathrm{nom}}$ and $v_{s,i}^{\mathrm{nom}}$, for $\mathrm{DG}_{s,i}$, and further regulate its terminal frequency and voltage outputs to the references, ω_s^{ref} and v_s^{ref}, provided by the tertiary control stage.

B. Model of Two-Layer Communication Network

The lower cyber network refers to the secondary control layer which contains M graphes, $\mathcal{G}_1$, $\mathcal{G}_2$, and $\mathcal{G}_M$, respectively corresponding to M MGs. For the sth MG, MG_s, its communication graph is defined as $\mathcal{G}_s(\mathcal{V}_s, \mathcal{E}_s, A_s)$, where the node set $\mathcal{V}_s = \{\mathcal{V}_1^s, \mathcal{V}_2^s, \cdots, \mathcal{V}_{m_s}^s\}$ represents all DGs within MG_s and the set of edges $\mathcal{E}_s \subseteq \mathcal{V}_s \times \mathcal{V}_s$ represents the communication links within MG_s. $A_s = (a_{ij}^s)_{m_s \times m_s}$ is an adjacency matrix with elements $a_{ii}^s = 0$ and $a_{ij}^s \geq 0$. $a_{ij}^s = 0$ if and only if the edge $(\mathcal{V}_i^s, \mathcal{V}_j^s) \in \mathcal{E}_s$. The neighbor set of $\mathrm{DG}_{s,i}$ (the ith DG within MG_s) is given by $N_{s,i} = \{\mathcal{V}_j^s \in \mathcal{V}_s : (\mathcal{V}_i^s, \mathcal{V}_j^s) \in \mathcal{E}_s\}$.

The upper cyber network refers to the tertiary control layer which is responsible to generate frequency/voltage references for the secondary control layer. Similarly, we define the desired graph as $\tilde{\mathcal{G}}(\tilde{\mathcal{V}}, \tilde{\mathcal{E}}, \tilde{A})$ with virtual node set $\tilde{\mathcal{V}} = \{\tilde{\mathcal{V}}_1, \tilde{\mathcal{V}}_2, \cdots, \tilde{\mathcal{V}}_M\}$ (representing different reference information states of M MGs), set of edges $\tilde{\mathcal{E}} \subseteq \tilde{\mathcal{V}} \times \tilde{\mathcal{V}}$ (representing the communication links among MGs), and adjacency matrix $\tilde{A} = (\tilde{a}_{s\tilde{k}})_{M\times M}$. Moreover, the neighbor set MG_s is $\tilde{N}_s = \{\tilde{\mathcal{V}}_{\tilde{k}} \in \tilde{\mathcal{V}} : (\tilde{\mathcal{V}}_s, \tilde{\mathcal{V}}_{\tilde{k}}) \in \tilde{\mathcal{E}}\}$.

To describe the information exchange between the upper network, $\tilde{\mathcal{G}}$, and the lower networks, $\{\mathcal{G}_s\}_{s\in\mathcal{I}_M}$, we introduce the leader-adjacency matrix $B_s = \mathrm{diag}\{a_{10}^s, \cdots, a_{m_s 0}^s\}$ for each MG_s, where $a_{i0}^s > 0$ ($i \in \mathcal{I}_{m_s}$) if follower-$\mathrm{DG}_{s,i}$ is connected to the virtual node MG_s across the pinning link $(\tilde{\mathcal{V}}_s, \mathcal{V}_i^s)$, otherwise $a_{i0}^s = 0$.

III. DHC Control Strategy for MG Clusters

The DHC strategy contains a pinning-based secondary DSC scheme and a consensus-based tertiary DTC scheme. The DTC scheme is responsible to generate frequency/voltage references for each MG according to the active/reactive power mismatch among MGs, with which the DSC scheme can then adjust the frequency/voltage nominal set-points for the primary control of each DG. Moreover, a pinning-based distributed cooperative control idea from multi-agent systems [29] is adopted here to reduce the number of controllers for the MGs with large number of DGs. Before proceeding the main results, we transform the MG cluster system into a discrete time system with different sampling periods for different control layers.

Time is discretized into a finite time sequence of nonempty and bounded intervals, $[t_k, t_{k+1})$ with $t_0 = 0$ and $k \in \bar{\mathcal{Z}}$, representing the kth round (secondary or tertiary control) iteration index, as shown in Fig. 2. We assume that there are totally τ^* (or T^*) times secondary (or tertiary, respectively) state update (iteration) in each time interval $[t_k, t_{k+1})$. To be specific, for the secondary control layer with sampling period τ_{sa}, there is a sequence of nonoverlapping subintervals $[t_k^0, t_k^1)$, $[t_k^1, t_k^2)$, $\cdots$, $[t_k^{\tau^*-1}, t_k^{\tau^*})$ with $t_k^0 = t_k, t_k^{\tau^*} = t_{k+1}$, satisfying $t_k^{\ell+1} - t_k^{\ell} = \tau_{\mathrm{sa}}$ for any non-negative integers k and ℓ; for the tertiary control layer with sampling period T_{sa}, there is a sequence of nonoverlapping subintervals $[t_k^{\tilde{0}}, t_k^{\tilde{1}})$, $\cdots$, $[t_k^{\tilde{\ell}}, t_k^{\tilde{\ell}+1})$, $\cdots$, $[t_k^{T^*-1}, t_k^{T^*})$ with $t_k^{\tilde{0}} = t_k, t_k^{T^*} = t_{k+1}$, satisfying $t_k^{\tilde{\ell}+1} - t_k^{\tilde{\ell}} = T_{\mathrm{sa}}$ for any non-negative integers k and $\tilde{\ell}$. Nevertheless, the secondary (or tertiary) inputs will be designed to only update at the end of the kth iterative process, i.e., $[t_k^{\tau^*}, t_k^{\tau^*} + \Delta\tau)$ with $\Delta\tau \ll \tau_{\mathrm{sa}}$ (or $[t_k^{T^*}, t_k^{T^*} + \Delta T)$ with

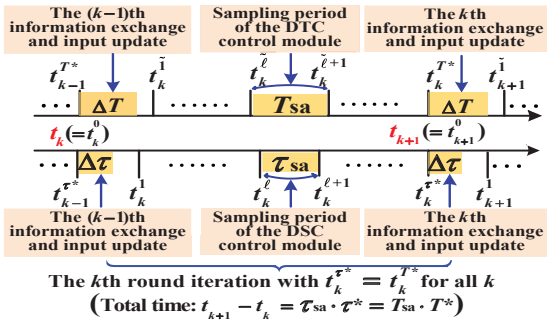

Fig. 2. Time diagram of the proposed DHC strategy.

$\Delta T \ll T_{\rm sa}$, respectively). For simplicity, we call τ^* and T^* the number of the secondary and tertiary input update in each round of the iteration, and $t_k^{\tau^*} = k\cdot\tau^*\cdot\tau_{\rm sa}$ and $t_k^{T^*} = k\cdot T^*\cdot T_{\rm sa}$ the terminal times of the system state outputs for secondary and tertiary control layers, respectively.

Remark 1: The assumption of $\tau^* \cdot \tau_{\rm sa} = T^* \cdot T_{\rm sa}$ is very mild since one can always choose the intervals, $[t_k, t_{k+1})$, to satisfy it. Moreover, since the tertiary layer is generally operating with a larger time scale than that of the secondary layer, their associated sampling periods are supposed to satisfy $T_{\rm sa} > \tau_{\rm sa}$. With a larger sampling period, the tertiary input update number is therefore shorter than that of the secondary layer, i.e., $T^* < \tau^*$, to ensure the same terminal time of the system state outputs for different control layers. The detailed constraints on these parameters will be derived later.

A. Local Droop-based Primary Control

Based on the traditional droop control strategy and the d-q reference frame transformation, where the d-axis and q-axis of the reference frame of each DG are rotating with the common reference frequency [13], the references of output d-axis voltage and frequency of $\text{DG}_{s,i}$ can be abstracted as

$$\begin{cases} \omega_{s,i}(t_k^\ell) = \omega_{s,i}^{\rm nom}(t_k^\ell) - K_{s,i}^P P_{s,i}(t_k^\ell), \\ v_{s,i}^{\rm od}(t_k^\ell) = v_{s,i}^{\rm nom}(t_k^\ell) - K_{s,i}^Q Q_{s,i}(t_k^\ell),\ v_{s,i}^{\rm oq}(t_k^\ell) = 0, \end{cases} \tag{1}$$

for $s \in \mathcal{I}_M$, $i \in \mathcal{I}_{m_s}$, $k \in \bar{\mathcal{Z}}$, and $\ell \in \mathcal{I}_{\tau^*}$, where $\omega_{s,i}^{\rm nom}$ and $v_{s,i}^{\rm nom}$ are respectively the nominal set-points of the frequency and d-axis actual output voltage, $\omega_{s,i}$ and $v_{s,i}^{\rm od}$. $P_{s,i}$ and $Q_{s,i}$ are the measured active and reactive powers with the associated droop coefficients, $K_{s,i}^P$ and $K_{s,i}^Q$. The voltage magnitude $v_{s,i} = \sqrt{\left(v_{s,i}^{\rm od}\right)^2 + \left(v_{s,i}^{\rm oq}\right)^2}$ with the d-axis and q-axis voltages $v_{s,i}^{\rm od}$ and $v_{s,i}^{\rm oq}$. Since primary voltage control is to align the voltage magnitude on the d-axis of its reference frame, $v_{s,i}^{\rm oq} = 0$ and we denote $v(t_k^\ell) = v^{\rm od}(t_k^\ell)$ for simplicity.

B. DSC Scheme for all DGs within MG_s

The discrete-time system states for the MG_s are updated as

$$\omega_{s,i}(t_k^{\ell+1}) = \omega_{s,i}(t_k^\ell) + u_{s,i}^\omega(k),\ v_{s,i}(t_k^{\ell+1}) = v_{s,i}(t_k^\ell) + u_{s,i}^v(k), \tag{2}$$

$$P_{s,i}(t_k^{\ell+1}) = P_{s,i}(t_k^\ell) + u_{s,i}^P(k),\ Q_{s,i}(t_k^{\ell+1}) = Q_{s,i}(t_k^\ell) + u_{s,i}^Q(k), \tag{3}$$

respectively with the voltage, frequency, active, and reactive power controllers, $u_{s,i}^\omega$, $u_{s,i}^v$, $u_{s,i}^P$, and $u_{s,i}^Q$.

We aim to tune the frequency and voltage of each $\text{DG}_{s,i}$, $\omega_{s,i}$ and $v_{s,i}$, to the references, $\omega_s^{\rm ref}$ and $v_s^{\rm ref}$ (provided by the tertiary control level), exactly at the terminal time $t_k^{\tau^*}$. Moreover, to obtain the accurate reactive power sharing in MGs with line impedances, a compromise scheme is to ensure the weighted average value of all DGs' output voltages within MG_s to converge to the desired reference value [13],[14]. Then, we will design the controllers in (2)-(3) so as to regulate the nominal set-points in (1), such that the system terminal outputs, $\omega_{s,i}(t_k^{\tau^*})$, $v_{s,i}(t_k^{\tau^*})$, $P_{s,i}(t_k^{\tau^*})$, and $Q_{s,i}(t_k^{\tau^*})$, satisfy

$$\lim_{k\to\infty}\left|\omega_{s,i}(t_k^{\tau^*}) - \omega_s^{\rm ref}\right| = 0,\ \lim_{k\to\infty}\left|\mu_{s,i}v_{s,i}(t_k^{\tau^*}) - v_s^{\rm ref}\right| = 0, \tag{4}$$

$$\begin{aligned} \lim_{k\to\infty}\left|P_{s,i}(t_k^{\tau^*})/P_{s,i}^{\max} - P_{s,j}(t_k^{\tau^*})/P_{s,j}^{\max}\right| = 0, \\ \lim_{k\to\infty}\left|Q_{s,i}(t_k^{\tau^*})/Q_{s,i}^{\max} - Q_{s,j}(t_k^{\tau^*})/Q_{s,j}^{\max}\right| = 0, \end{aligned} \tag{5}$$

for all $i \neq j \in \mathcal{I}_{m_s}$ and $s \in \mathcal{I}_M$, where $P_{s,i}^{\max}$ and $Q_{s,i}^{\max}$ are the instantaneous maximum capacities of the active and reactive powers of $\text{DG}_{s,i}$, respectively, $\mu_s = (\mu_{s,1}, \cdots, \mu_{s,m_s})^T \in R^{m_s}$ is the positive left eigenvector corresponding to the zero eigenvalue of the Laplacian matrix (associated with the graph $\mathcal{G}_s$ of MG_s). $\mu_s = (1/m_s, \cdots, 1/m_s)^T$ if $\mathcal{G}_s$ is undirected.

1) DSC Scheme for Voltage and Frequency Regulation: We firstly design the following distributed voltage observer to estimate each DG's voltage, $v_{s,i}$, and then pin the estimation, $\hat{v}_{s,i}$, to the voltage reference, $v_s^{\rm ref}$.

$$\begin{aligned} \hat{v}_{s,i}(t_k^{\ell+1}) = &\textstyle\sum_{j\in N_{s,i}} \gamma_{ij}^s a_{ij}^s[\hat{v}_{s,j}(t_k^\ell) - \hat{v}_{s,i}(t_k^\ell)] \\ &+[v_{s,i}(t_k^{\ell+1}) - v_{s,i}(t_k^\ell)] + \hat{v}_{s,i}(t_k^\ell), \end{aligned} \tag{6}$$

where $v_{s,i}(t_k^\ell)$ and $\hat{v}_{s,i}(t_k^\ell)$ are respectively the measured voltage and voltage estimation of $\text{DG}_{s,i}$ at time t_k^ℓ, the associated neighbor set $N_{s,i}$ and adjacency matrix $A_s = (a_{ij}^s)_{m_s\times m_s}$ are defined previously, and $\Gamma_s = (\gamma_{ij}^s)_{m_s\times m_s}$ is the gain matrix.

By the proof in Appendix, the observer (6) can drive each DG's voltage estimation to converge to the weighted average voltage value of all DGs within MG_s if $\mathcal{G}_s$ is connected.

Now we design $u_{s,i}^\omega$ and $u_{s,i}^v$ using the information of relative terminal outputs between neighboring DGs:

$$\begin{cases} u_{s,i}^\omega(k+1) = \gamma_{i0}^s a_{i0}^s[\omega_s^{\rm ref}(t_k^{\tau^*}) - \omega_{s,i}(t_k^{\tau^*})] \\ \quad + \sum_{j\in N_{s,i}} \gamma_{ij}^s a_{ij}^s[\omega_{s,j}(t_k^{\tau^*}) - \omega_{s,i}(t_k^{\tau^*})], \\ u_{s,i}^v(k+1) = \gamma_{i0}^s a_{i0}^s[v_s^{\rm ref}(t_k^{\tau^*}) - \hat{v}_{s,i}(t_k^{\tau^*})], \end{cases} \tag{7}$$

with the leader adjacency matrix $B_s = \text{diag}\{a_{10}^s, \cdots, a_{m_s0}^s\}$ and the gain matrix $\Xi_s = \text{diag}\{\gamma_{10}^s, \cdots, \gamma_{m_s0}^s\}$. $\text{DG}_{s,i}$ can access $\omega_s^{\rm ref}$ and $v_s^{\rm ref}$ if and only if $b_{i,0}^s > 0$, i.e., $\text{DG}_{s,i}$ is selected as one of the pinned-DGs within MG_s. Denote the index $(s,i) \in (s, \text{pin})$ with $\text{pin} \subset \mathcal{I}_{m_s}$ and $i \in \text{pin}$.

2) DSC Scheme for Active and Reactive Power Sharing: The power outputs are expected to achieve power sharing proportionally to DG's capacities in the steady state, i.e.,

$$\begin{aligned} P_{s,i}(t_k^{\tau^*})/P_{s,i}^{\max} = P_{s,j}(t_k^{\tau^*})/P_{s,j}^{\max}, \\ Q_{s,i}(t_k^{\tau^*})/Q_{s,i}^{\max} = Q_{s,j}(t_k^{\tau^*})/Q_{s,j}^{\max}, \end{aligned} \tag{8}$$

for all $i \neq j \in \mathcal{I}_{m_s}$. Since the droop coefficients, $K_{s,i}^P$ and $K_{s,i}^Q$, are generally selected based on the maximum capacities of active and reactive power, $P_{s,i}^{\max}$ and $Q_{s,i}^{\max}$, so as to satisfy

$$K_{s,j}^P/P_{s,i}^{\max} = K_{s,i}^P/P_{s,j}^{\max},\ K_{s,j}^Q/Q_{s,i}^{\max} = K_{s,i}^Q/Q_{s,j}^{\max}, \tag{9}$$

we then design the consensus-based power controllers:

$$\begin{cases} u_{s,i}^P(k+1) = \sum\limits_{j\in N_{s,i}} \gamma_{ij}^s a_{ij}^s[K_{s,j}^P P_{s,j}(t_k^{\tau^*}) - K_{s,i}^P P_{s,i}(t_k^{\tau^*})]/K_{s,i}^P, \\ u_{s,i}^Q(k+1) = \sum\limits_{j\in N_{s,i}} \gamma_{ij}^s a_{ij}^s[K_{s,j}^Q Q_{s,j}(t_k^{\tau^*}) - K_{s,i}^Q Q_{s,i}(t_k^{\tau^*})]/K_{s,i}^Q. \end{cases} \tag{10}$$

With the DSC controllers (7) and (10), the nominal set-points of frequency and voltage for $\text{DG}_{s,i}$ can be updated as

$$\begin{cases} \omega_{s,i}^{\rm nom}(t_k^{\ell+1}) = \omega_{s,i}^{\rm nom}(t_k^\ell) + u_{s,i}^\omega(k) + K_{s,i}^P u_{s,i}^P(k), \\ v_{s,i}^{\rm nom}(t_k^{\ell+1}) = v_{s,i}^{\rm nom}(t_k^\ell) + u_{s,i}^v(k) + K_{s,i}^Q u_{s,i}^Q(k), \end{cases} \tag{11}$$

which will be used to further regulate the frequency/voltage by the power control loop in the primary stage.

C. DTC Scheme for Power Sharing among Multiple MGs

The tertiary control level aims to adjust the power flow among MGs to achieve the power outputs balance, i.e.,

$$\begin{cases} \lim\limits_{k\to+\infty}\left|\tilde{P}_s(t_k^{T^*})/\tilde{P}_s^{\max}-\tilde{P}_{\tilde{k}}(t_k^{T^*})/\tilde{P}_{\tilde{k}}^{\max}\right|=0,\\ \lim\limits_{k\to+\infty}\left|\tilde{Q}_s(t_k^{T^*})/\tilde{Q}_s^{\max}-\tilde{Q}_{\tilde{k}}(t_k^{T^*})/\tilde{Q}_{\tilde{k}}^{\max}\right|=0 \end{cases} \tag{12}$$

for all $s\neq\tilde{k}\in\mathcal{I}_M$, where $\tilde{P}_s$ ($\tilde{Q}_s$) and $\tilde{P}_s^{\max}$ ($\tilde{Q}_s^{\max}$) respectively denote the total active (reactive) power outputs and the associated maximum capacities of MG_s.

Assume only one DG, denoted as $\mathrm{DG}_{s,\mathrm{pin}}$, can be pinned for each MG_s, then $\mathrm{pin}\in\mathcal{I}_{m_s}$. By the objective (5), the tertiary power sharing objective (12) will be achieved if

$$\begin{cases} \lim\limits_{k\to+\infty}\left|P_{s,\mathrm{pin}}(t_k^{T^*})/P_{s,\mathrm{pin}}^{\max}-P_{\tilde{k},\mathrm{pin}}(t_k^{T^*})/P_{\tilde{k},\mathrm{pin}}^{\max}\right|=0,\\ \lim\limits_{k\to+\infty}\left|Q_{s,\mathrm{pin}}(t_k^{T^*})/Q_{s,\mathrm{pin}}^{\max}-Q_{\tilde{k},\mathrm{pin}}(t_k^{T^*})/Q_{\tilde{k},\mathrm{pin}}^{\max}\right|=0 \end{cases} \tag{13}$$

for all $s\neq\tilde{k}\in\mathcal{I}_M$, where $P_{s,\mathrm{pin}}$ ($Q_{s,\mathrm{pin}}$) and $P_{s,\mathrm{pin}}^{\max}$ ($Q_{s,\mathrm{pin}}^{\max}$) are respectively the active (reactive) power outputs and the associated maximum capacities of $\mathrm{DG}_{s,\mathrm{pin}}$. Now the consensus-based DTC controller can be designed as

$$\begin{cases} P_{s,\mathrm{pin}}(t_k^{\tilde{\ell}+1})=P_{s,\mathrm{pin}}(t_k^{\tilde{\ell}})+\tilde{u}_{s,\mathrm{pin}}^P(k),\\ Q_{s,\mathrm{pin}}(t_k^{\tilde{\ell}+1})=Q_{s,\mathrm{pin}}(t_k^{\tilde{\ell}})+\tilde{u}_{s,\mathrm{pin}}^Q(k), \end{cases} \tag{14}$$

with the discrete time control inputs

$$\begin{cases} \tilde{u}_{s,\mathrm{pin}}^P(k+1)=\sum_{\tilde{k}\in\tilde{N}_s}\tilde{\gamma}_{s\tilde{k}}\tilde{a}_{s\tilde{k}}[K_{\tilde{k},\mathrm{pin}}^P P_{\tilde{k},\mathrm{pin}}(t_k^{T^*})\\ \qquad -K_{s,\mathrm{pin}}^P P_{s,\mathrm{pin}}(t_k^{T^*})]/K_{s,\mathrm{pin}}^P,\\ \tilde{u}_{s,\mathrm{pin}}^Q(k+1)=\sum_{\tilde{k}\in\tilde{N}_s}\tilde{\gamma}_{s\tilde{k}}\tilde{a}_{s\tilde{k}}[K_{\tilde{k},\mathrm{pin}}^Q Q_{\tilde{k},\mathrm{pin}}(t_k^{T^*})\\ \qquad -K_{s,\mathrm{pin}}^Q Q_{s,\mathrm{pin}}(t_k^{T^*})]/K_{s,\mathrm{pin}}^Q, \end{cases} \tag{15}$$

for $\tilde{\ell}\in\bar{\mathcal{I}}_{T^*}$, $s\in\mathcal{I}_M$, and $\mathrm{pin}\in\mathcal{I}_{m_s}$, where $K_{s,\mathrm{pin}}^P$ and $K_{s,\mathrm{pin}}^Q$ are respectively the droop coefficients of $\mathrm{DG}_{s,\mathrm{pin}}$, $\tilde{A}=(\tilde{a}_{ij})_{M\times M}$ is the adjacency matrix of network graph $\tilde{\mathcal{G}}$ (see Fig. 1). $\tilde{\Gamma}=(\tilde{\gamma}_{s\tilde{k}})_{M\times M}$ is the associated gain matrix.

By integrating the power flow mismatch among MGs across $\tilde{\mathcal{G}}$, the final references, ω_s^{ref} and v_s^{ref}, for MG_s can be set as

$$\begin{cases} \omega_s^{\mathrm{ref}}(t_k^{T^*})=\omega^{\mathrm{rated}}+K_{s,\mathrm{pin}}^P P_{s,\mathrm{pin}}(t_k^{T^*}),\\ v_s^{\mathrm{ref}}(t_k^{T^*})=v^{\mathrm{rated}}+K_{s,\mathrm{pin}}^Q Q_{s,\mathrm{pin}}(t_k^{T^*}), \end{cases} \tag{16}$$

where ω^{rated} and v^{rated} are respectively the rated frequency and voltage of the MG cluster system.

Remark 2: $u_{s,i}^P$ and $u_{s,i}^Q$ in (11) are the secondary control inputs of all $\mathrm{DG}_{s,i}$ ($i\in\mathcal{I}_{m_s}$) within MG_s, while $\tilde{u}_{s,\mathrm{pin}}^P$ and $\tilde{u}_{s,\mathrm{pin}}^Q$ in (14) are the tertiary control inputs of the pinth DG (i.e., $\mathrm{DG}_{s,\mathrm{pin}}$) within MG_s. In this sense, only $\mathrm{DG}_{s,\mathrm{pin}}$ within each MG_s is involved in the two-layer dynamics regulation.

Now the diagram of the DHC framework can be drawn in Fig. 3. As seen, the secondary cyber network $\mathcal{G}_s$ is responsible for exchanging the measured information of each $\mathrm{DG}_{s,i}$ within MG_s to generate the nominal set-points, $\omega_{s,i}^{\mathrm{nom}}$ and $v_{s,i}^{\mathrm{nom}}$ for the primary level. While the tertiary cyber network $\tilde{\mathcal{G}}$ is responsible for transmitting the measured information of each pinned $\mathrm{DG}_{s,\mathrm{pin}}$ from each MG_s to the tertiary level to further generate the references, ω_s^{ref} and v_s^{ref}, to the secondary level. For each MG_s, the power outputs of the pinned $\mathrm{DG}_{s,\mathrm{pin}}$, $P_{s,\mathrm{pin}}$ and $Q_{s,\mathrm{pin}}$, possess both secondary and tertiary control dynamics, (10) and (15), with different sampling periods, τ_{sa} and T_{sa}, and terminal times, τ^* and T^*. Since the response times for different layers should match each other, we next present the stability analysis.

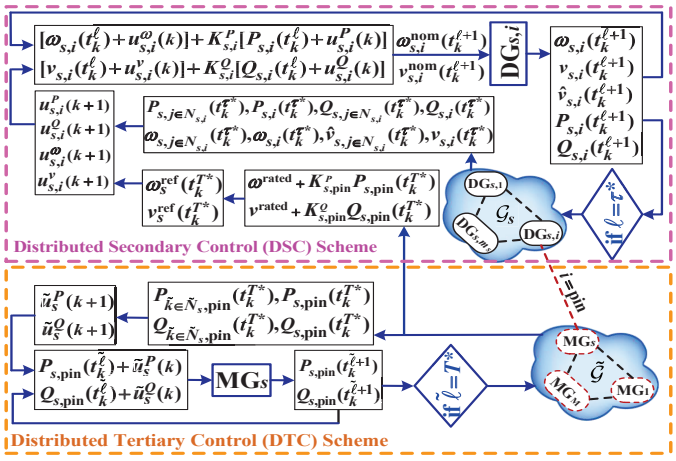

Fig. 3. The block diagram of the DHC framework for AC MG clusters.

IV. Stability Analysis of the MG Cluster System

To facilitate the mathematical representation, let the number of DGs within each MG be always equal to m, i.e., $m_1=\cdots=m_M=m$. However, the general case can be analyzed similarly. For the variables in the secondary level, let the states $\omega_s=(\omega_{s,1},\cdots,\omega_{s,m})^T$, $v_s=(v_{s,1},\cdots,v_{s,m})^T$, $\hat{v}_s=(\hat{v}_{s,1},\cdots,\hat{v}_{s,m})^T$, $p_s=(p_{s,1},\cdots,p_{s,m})^T$, $q_s=(q_{s,1},\cdots,q_{s,m})^T$, the inputs $u_s^\omega=(u_{s,1}^\omega,\cdots,u_{s,m}^\omega)^T$, $u_s^v=(u_{s,1}^v,\cdots,u_{s,m}^v)^T$, $u_s^P=(K_{s,1}^P u_{s,1}^P,\cdots,K_{s,m}^P u_{s,m}^P)^T$, and $u_s^Q=(K_{s,1}^Q u_{s,1}^Q,\cdots,K_{s,m}^Q u_{s,m}^Q)^T$, moreover, denote $p_{s,i}=K_{s,i}^P P_{s,i}$, and $q_{s,i}=K_{s,i}^Q Q_{s,i}$. For the variables in the tertiary level, let the states $p_{\mathrm{pin}}=(p_{1,\mathrm{pin}},\cdots,p_{M,\mathrm{pin}})^T$, $q_{\mathrm{pin}}=(q_{1,\mathrm{pin}},\cdots,q_{M,\mathrm{pin}})^T$, the inputs $\tilde{u}_{\mathrm{pin}}^P=(K_{1,\mathrm{pin}}^P\tilde{u}_{1,\mathrm{pin}}^P,\cdots,K_{M,\mathrm{pin}}^P\tilde{u}_{M,\mathrm{pin}}^P)^T$, and $\tilde{u}_{\mathrm{pin}}^Q=(K_{1,\mathrm{pin}}^Q\tilde{u}_{1,\mathrm{pin}}^Q,\cdots,K_{M,\mathrm{pin}}^Q\tilde{u}_{M,\mathrm{pin}}^Q)^T$. Denote $\omega=(\omega_1^T,\cdots,\omega_M^T)^T$, $v=(v_1^T,\cdots,v_M^T)^T$, $\hat{v}=(\hat{v}_1^T,\cdots,\hat{v}_M^T)^T$, $p=(p_1^T,\cdots,p_M^T)^T$, $q=(q_1^T,\cdots,q_M^T)^T$, $B=\mathrm{diag}\{B_1,\cdots,B_M\}$, and $\Xi=\mathrm{diag}\{\Xi_1,\cdots,\Xi_M\}$ with $\Xi_s=\mathrm{diag}\{\gamma_{10}^s,\cdots,\gamma_{m0}^s\}$. Finally, define the Laplacian matrices $L_s=(\ell_{ij}^s)_{m\times m}$ and $\tilde{L}=(\tilde{\ell}_{s\times\tilde{k}})_{M\times M}$ respectively as

$$\ell_{ij}^s=\begin{cases}\sum\limits_{q\in N_{s,j}}a_{iq}^s\gamma_{iq}^s, & j=i,\\ -a_{ij}^s\gamma_{ij}^s, & j\neq i,\end{cases}\qquad \tilde{\ell}_{s\tilde{k}}=\begin{cases}\sum\limits_{\tilde{k}\in\tilde{N}_s}\tilde{a}_{s\tilde{k}}^s\tilde{\gamma}_{s\tilde{k}}^s, & \tilde{k}=s,\\ -\tilde{a}_{s\tilde{k}}\tilde{\gamma}_{s\tilde{k}}, & \tilde{k}\neq s\end{cases}$$

with gain matrices $\Gamma_s=(\gamma_{i,j}^s)_{i,j=1}^m$ and $\tilde{\Gamma}=(\tilde{\gamma}_{s,\tilde{k}})_{s,\tilde{k}=1}^m$ to be designed later. Let $L=\mathrm{diag}\{L_1,\cdots,L_M\}$, the dynamics,

This article has been accepted for publication in a future issue of this journal, but has not been fully edited. Content may change prior to final publication. Citation information: DOI 10.1109/TII.2017.2783334, IEEE Transactions on Industrial Informatics

(2), (3), (7), (10), (14), and (15), can be rewritten as

$$\begin{cases} \omega(t_{k+1}^{\tau^*}) = [I_{Mm} - \tau^*(L + B \odot \Xi)]\omega(t_k^{\tau^*}) \\ \qquad +\tau^*(B \odot \Xi)[\omega^{\rm rated} 1_{Mm} + p_{\rm pin}(t_k^{T^*})1_m], \\ \hat{v}(t_{k+1}^{\tau^*}) = [I_{Mm} - \tau^*(L + B \odot \Xi)]\hat{v}(t_k^{\tau^*}) \\ \qquad +\tau^*(B \odot \Xi)[v^{\rm rated} 1_{Mm} + q_{\rm pin}(t_k^{T^*})1_m], \\ p(t_{k+1}^{\tau^*}) = [I_{Mm} - \tau^* L]p(t_k^{\tau^*}), \\ q(t_{k+1}^{\tau^*}) = [I_{Mm} - \tau^* L]q(t_k^{\tau^*}), \\ p_{\rm pin}(t_{k+1}^{T^*})1_m = [I_{Mm} - T^*(\tilde{L} \otimes I_m)]p_{\rm pin}(t_k^{T^*})1_m, \\ q_{\rm pin}(t_{k+1}^{T^*})1_m = [I_{Mm} - T^*(\tilde{L} \otimes I_m)]q_{\rm pin}(t_k^{T^*})1_m. \end{cases} \tag{17}$$

Let $\tilde{\mu} = (\frac{1}{M}, ..., \frac{1}{M}) \in \mathrm{R}^M$, being the positive left eigenvector corresponding to the zero eigenvalue of $\tilde{L}$, denote the error variables $\bar{\omega} = \omega - (\omega^{\rm rated} 1_{Mm} + p_{\rm pin} 1_m)$, $\bar{v} = \hat{v} - (v^{\rm rated} 1_{Mm} + q_{\rm pin} 1_m)$, $\bar{p}_{\rm pin} 1_m = p_{\rm pin} 1_m - \tilde{\mu}^T p_{\rm pin}(0) 1_m$, and $\bar{q}_{\rm pin} 1_m = q_{\rm pin} 1_m - \tilde{\mu}^T q_{\rm pin}(0) 1_m$, the error dynamics

$$\begin{cases} \bar{\omega}(t_{k+1}^{\tau^*}) = [I_{Mm} - \tau^*(L + B \odot \Xi)]\bar{\omega}(t_k^{\tau^*}) \\ \qquad +T^*(\tilde{L} \otimes I_m)\bar{p}_{\rm pin}(t_k^{T^*})1_m, \\ \bar{v}(t_{k+1}^{\tau^*}) = [I_{Mm} - \tau^*(L + B \odot \Xi)]\bar{v}(t_k^{\tau^*}) \\ \qquad +T^*(\tilde{L} \otimes I_m)\bar{q}_{\rm pin}(t_k^{T^*})1_m, \\ \bar{p}(t_{k+1}^{\tau^*}) = [I_{Mm} - \tau^* L]\bar{p}(t_k^{\tau^*}) + T^*(\tilde{L} \otimes I_m)\bar{p}_{\rm pin}(t_k^{T^*})1_m, \\ \bar{q}(t_{k+1}^{\tau^*}) = [I_{Mm} - \tau^* L]\bar{q}(t_k^{\tau^*}) + T^*(\tilde{L} \otimes I_m)\bar{q}_{\rm pin}(t_k^{T^*})1_m, \\ \bar{p}_{\rm pin}(t_{k+1}^{T^*})1_m = [I_{Mm} - T^*(\tilde{L} \otimes I_m)]\bar{p}_{\rm pin}(t_k^{T^*})1_m, \\ \bar{q}_{\rm pin}(t_{k+1}^{T^*})1_m = [I_{Mm} - T^*(\tilde{L} \otimes I_m)]\bar{q}_{\rm pin}(t_k^{T^*})1_m, \end{cases} \tag{18}$$

Denote $z_k = ([\bar{p}_{\rm pin}(t_k^{T^*})1_m]^T, [\bar{q}_{\rm pin}(t_k^{T^*})1_m]^T)^T$, $x_k = ([\bar{\omega}(t_k^{\tau^*})]^T, [\bar{v}(t_k^{\tau^*})]^T)^T$, $y_k = ([\bar{p}(t_k^{\tau^*})]^T, [\bar{q}(t_k^{\tau^*})]^T)^T$, then (18) can be rewritten as

$$\begin{cases} x_{k+1} = \Phi x_k + (I_{2Mm} - \Omega) z_k, \\ y_{k+1} = \Psi y_k + (I_{2Mm} - \Omega) z_k, \\ z_{k+1} = \Omega z_k, \end{cases} \tag{19}$$

where $\Phi = I_2 \otimes [I_{Mm} - \tau^*(L + B \odot \Xi)]$, $\Psi = I_2 \otimes [I_{Mm} - \tau^* L]$, and $\Omega = I_2 \otimes [I_{Mm} - T^*(\tilde{L} \otimes I_m)]$ are all symmetric matrices.

We next claim the stability of the origin of the error system (19). Define the Lyapunov candidates

$$V_k(x_k, y_k, z_k) = x_k^T x_k + y_k^T y_k + z_k^T z_k, \tag{20}$$

and difference along the trajectory of system (20), we have

$$\Delta V_k = V_{k+1} - V_k \le (x_k^T, y_k^T, z_k^T) S (x_k^T, y_k^T, z_k^T)^T \tag{21}$$

for a blocking matrix $S = \mathrm{diag}\{S_1, S_2, S_3\}$ with $S_1 = (1 + \frac{1}{\theta})\Phi^2 - I_{2Mm}$, $S_2 = (1 + \frac{1}{\theta})\Psi^2 - I_{2Mm}$, $S_3 = \Omega^2 + (2 + 2\theta)(I_{2Mm} - \Omega)^2 - I_{2Mm}$, and any positive constant $\theta > 0$. By the special matrix theory [30] and the symmetry of matrices Φ, Ψ, and Ω, a sufficient condition for $\Delta V_k < 0$ is

$$\begin{cases} (1 + \frac{1}{\theta})\lambda_{2Mm}^2(\Phi) < 1, \ (1 + \frac{1}{\theta})\lambda_{2M(m-1)}^2(\Psi) < 1, \\ \max\limits_{1 \le i \le 2(M-1)m} \lambda_i^2(\Omega) + (2 + 2\theta)[1 - \lambda_i(\Omega)]^2 < 1, \end{cases} \tag{22}$$

which leads to

$$\max\{\frac{\lambda_{2Mm}^2(\Phi)}{1 - \lambda_{2Mm}^2(\Phi)}, \frac{\lambda_{2M(m-1)}^2(\Psi)}{1 - \lambda_{2M(m-1)}^2(\Psi)}\} < \theta < \frac{3\lambda_1(\Omega) - 1}{2[1 - \lambda_1(\Omega)]} \tag{23}$$

for a certain positive constant θ provided that $\lambda_{2Mm}(\Phi) < 1$, $\lambda_{2M(m-1)}(\Psi) < 1$, and $\frac{1}{3} < \lambda_1(\Omega) \le \lambda_{2(M-1)m}(\Omega) < 1$. Thus, by the previous denotations we obtain that

$$\begin{cases} \lambda_{2Mm}(\Phi) = 1 - \tau^* \lambda_1(L + B \odot \Xi), \\ \lambda_{2M(m-1)}(\Psi) = 1 - \tau^* \lambda_{M+1}(L), \\ \lambda_{2(M-1)m}(\Omega) = 1 - T^* \lambda_2(\tilde{L}), \ \lambda_1(\Omega) = 1 - T^* \lambda_M(\tilde{L}), \end{cases} \tag{24}$$

By Gershgorin circle theorem [20], the above inequalities hold if the gain matrices and terminal times are selected such that

$$\begin{cases} \tau^* \sum_{j \in N_{s,i}} (\gamma_{ij}^s a_{ij}^s + \gamma_{i0}^s a_{i0}^s) < 1, \\ T^* \sum_{\tilde{k} \in \tilde{N}_s} \tilde{\gamma}_{s\tilde{k}} \tilde{a}_{s\tilde{k}} < 2/3, \end{cases} \tag{25}$$

$$\frac{\tau_{\rm sa}}{T_{\rm sa}} = \frac{T^*}{\tau^*} < \min\Big\{ \frac{\lambda_1(L + B \odot \Xi)[2 - \tau^* \lambda_1(L + B \odot \Xi)]}{\lambda_M(\tilde{L})}, \frac{\lambda_{M+1}(L)[2 - \tau^* \lambda_{M+1}(L)]}{\lambda_M(\tilde{L})} \Big\}. \tag{26}$$

Conclusion 1: If the two-layer communication networks, $\{\mathcal{G}_s\}_{s \in \mathcal{I}_M}$ and $\tilde{\mathcal{G}}$, are connected, and the associated numbers of the input update during each round of the iteration, T^* and τ^*, and the sampling periods, $T_{\rm sa}$ and $\tau_{\rm sa}$, of the tertiary and secondary control levels satisfy (25) and (26), then both of the secondary control objectives (4)-(5) and the tertiary control objective (13) can be achieved provided that at least one $\mathrm{DG}_{s,\rm pin}$ from each MG_s can be pinned to realized the information exchange among all the pinned DGs (in the tertiary level) and transmit the frequency and voltage references, $\omega_s^{\rm ref}$ and $v_s^{\rm ref}$, to its neighboring DGs within MG_s (in the secondary level).

The selected gain matrices, Γ_s, Ξ_s, and $\tilde{\Gamma}$, should not break the original network topologies. For example, all entries of Γ_s are always selected to satisfy $\gamma_{ij}^s = \gamma_{ji}^s > 0$ when $N_{s,i} \neq \emptyset$ and $j \in N_{s,i}$, otherwise $\gamma_{ij}^s = \gamma_{ji}^s = 0$. Other gain matrices also own the same requirements. Moreover, as illustrated in Remark 1, the assumption of $\tau^* \cdot \tau_{\rm sa} = T^* \cdot T_{\rm sa}$ with $\tau_{\rm sa} < T_{\rm sa}$ leads to $T^* < \tau^*$. Thus, we initialize all gain matrices as the associated adjacency matrices, and T^* as half of τ^*, and then further optimize their values by Algorithm 1.

Algorithm 1 Calculate parameters Γ_s, Ξ_s, $\tilde{\Gamma}$, and T^*.

Initialization:

Set $\varepsilon \in (0, 1)$, number of secondary input update τ^*, and let $\{(\gamma_{ij}^s)_{i,j=1}^{m_s}, (\gamma_{i0}^s)_{i=0}^{m_s}\}_{s=1}^M \to \{(a_{ij}^s)_{i,j=1}^{m_s}, (a_{i0}^s)_{i=0}^{m_s}\}_{s=1}^M$, $\{(\tilde{\gamma}_{s\tilde{k}})_{s,\tilde{k}=1}^M\} \to \{(\tilde{a}_{s\tilde{k}})_{s,\tilde{k}=1}^M\}$, and $T^* \to \lceil 0.5\tau^* \rceil$;

Iterative:

1: **while** inequality conditions in (25) do not hold **do** $\{(\gamma_{ij}^s)_{i,j=1}^{m_s}, (\gamma_{i0}^s)_{i=0}^{m_s}\} \leftarrow \varepsilon\{(\gamma_{ij}^s)_{i,j=1}^{m_s}, (\gamma_{i0}^s)_{i=0}^{m_s}\}$ for $s = 1, \cdots, m_s$, and $(\tilde{\gamma}_{s\tilde{k}})_{s,\tilde{k}=1}^M \leftarrow \varepsilon(\tilde{\gamma}_{s\tilde{k}})_{s,\tilde{k}=1}^M$;

2: **end while**

3: **while** inequality conditions in (26) do not hold **do** $T^* \leftarrow \max\{\lfloor \varepsilon T^* \rfloor, 1\}$;
  if $T^* = 1$ **do** $(\tilde{\gamma}_{s\tilde{k}})_{s,\tilde{k}=1}^M \leftarrow \varepsilon(\tilde{\gamma}_{s\tilde{k}})_{s,\tilde{k}=1}^M$;
  end if

4: **end while**

Set $\{\Gamma_s, \Xi_s, \tilde{\Gamma}, T^*\} \to \{(\gamma_{ij}^s)_{i,j=1}^{m_s}, (\gamma_{i0}^s)_{i=0}^{m_s}, (\tilde{\gamma}_{s\tilde{k}})_{s,\tilde{k}=1}^M, T^*\}$.

The coefficient $\varepsilon \in (0, 1)$ characterizes the changing rate of the gain matrices to achieve optimal values satisfying (25)

This article has been accepted for publication in a future issue of this journal, but has not been fully edited. Content may change prior to final publication. Citation information: DOI 10.1109/TII.2017.2783334, IEEE Transactions on Industrial Informatics

and (26). With the calculated numbers of the two-layer control input update, T^* and τ^*, one can obtain the sampling period ratio, $\tau_{\rm sa}/T_{\rm sa}$, according to (26), thus $T_{\rm sa}$ can be then designed for some given $\tau_{\rm sa}$.

Under the DHC framework shown in Fig. 3, the detailed implementation can be designed as follows:

Step 1: **Initialization:** Set the reference trajectory $v^{\rm rated}$ and $\omega^{\rm rated}$, the initial secondary and tertiary inputs $u_s^{\omega,v,P,Q}(0)$ and $\tilde{u}_{\rm pin}^{P,Q}(0)$, the related initial states, and the parameter τ^*. Let the iteration index $k=1$ and the tolerance ϵ_1 and ϵ_2.

Step 2: **Calculate gain matrices:**Determine Γ_s, Ξ_s, $\tilde{\Gamma}$, and T^*, according to Algorithm 1.

Step 3: **Calculate nominal set points:** Apply $\tilde{u}_{\rm pin}^{P,Q}(k)$ to compute $\omega_s^{\rm ref}(t_k^{\tilde{\ell}^*})$ and $v_s^{\rm ref}(t_k^{\tilde{\ell}^*})$; apply $u_s^{\omega,v,P,Q}(k)$ to compute $\omega_{s,i}^{\rm nom}(t_k^{\ell})$ and $v_{s,i}^{\rm nom}(t_k^{\ell})$ for $\tilde{\ell}\in\bar{\mathcal{I}}_{T^*}$, $\ell\in\bar{\mathcal{I}}_{\tau^*}$, $i\in\mathcal{I}_{m_s}$, and $s\in\mathcal{I}_M$.

Step 4: **Measure terminal outputs:** Apply $\omega_s^{\rm ref}(t_k^{T^*})$ and $v_s^{\rm ref}(t_k^{T^*})$ to the secondary layer and measure the terminal outputs, $\omega_{s,i}^{\rm nom}(t_k^{\tau^*})$ and $v_{s,i}^{\rm nom}(t_k^{\tau^*})$; which will be applied to the primary control process and measure the terminal outputs, $\omega_{s,i}(t_k^{\tau^*})$, $v_{s,i}(t_k^{\tau^*})$, $P_{s,i}(t_k^{\tau^*})$, and $Q_{s,i}(t_k^{\tau^*})$ for $i\in\mathcal{I}_{m_s}$ and $s\in\mathcal{I}_M$.

Step 5: **Analyze errors:** If Equation (4) holds with tolerance ϵ_1 and Equation (12) holds with tolerance ϵ_2, then go to step 7; Otherwise go to step 6.

Step 6: **Calculate control inputs:** Let $k=k+1$, and update $u_s^{\omega,v,P,Q}(k)$ and $\tilde{u}_{\rm pin}^{P,Q}(k)$ according to the protocols (7), (10), and (15), then go to step 3.

Step 7: Stop the iteration.

Remark 3: By introducing the concepts of interval weights and interval adjacency matrices [15], the proposed DHC strategy is also robust against the uncertain communication links caused by the internal uncertainties and/or external disturbances by minor change the inequalities (26) and (27).

Remark 4: When the frequency/voltage in each islanded MG cannot be retained within the acceptable limits by adjusting the set-points of generators or by controlling the power injection/absorption of energy storage systems, then the power mismatch signal between the MG will be detected. Simultaneously, the pinning control scheme will be implemented. In this situation, we can control the pinning instant by activating the corresponding communication links. Through adjusting the frequency and voltage of the pinned DGs across the tie-line, the power transfer among MGs can be finally realized.

Remark 5: Since different control variables possess different communication networks due to their different response times, it may be more practical to establish different communication networks for the information interaction of frequency and voltage, and the associated work can be found in [13]. Moreover, to stabilize the power outputs in a longer time scale than that of the frequency response, an alternative solution is to design a multiple time-scale control strategy by partially extending the results of [14],[29]. Additionally, in our control strategy, the sampling time of each layer communication network is not directly related to the dynamical evolution time of each actual physical module. For example, the evolution speed of the active power outputs depends on its frequency reference signal. Due to the slower dynamics of the active power, its final frequency reference will remain unchanged for a long period of time regardless of how fast the signal is collected in the communication network.

Remark 6: In view of the advantages of pinning control, the adopted pinning-based DSC scheme can greatly reduce the number of the controlled DGs in the lower network. While for the upper network, each pinned DG possesses a peer-to-peer attribute, thus a consensus-based DTC scheme is more suitable to realize a completely distributed control performance.

Remark 7: On one hand, the distributed network of public utility can benefit from the proposed DHC framework to achieve effectively monitor and control a large number of DGs in the overall network; on the other hand, the proposed DHC framework can also support demand-side management to increase the reliability of multiple MGs. In view of this, the proposed DHC framework will provide reference and guidance on the management of the scalability and controllability of large-scale DG access in distribution network for the distributed network of public utility and consumer.

V. Performance Validation

The effectiveness of the DHC strategy will be verified by simulating an AC MG cluster in Simulink/SimPowerSystems. The basic diagram of the AC MG cluster test system is shown in Fig. 4, and the specifications of the DGs, lines,

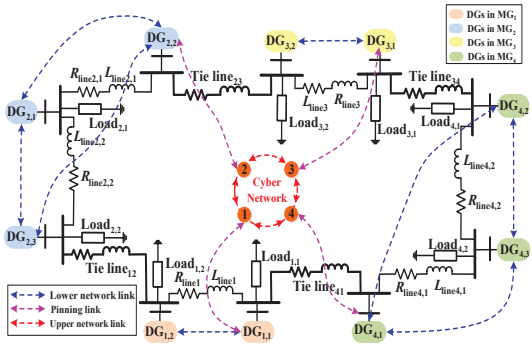

Fig. 4. Single line diagram of the DGs and loads in an AC MG cluster.

and loads are summarized in Table I. The rated frequency and terminal voltage magnitude of MGs, $\omega^{\rm rated}$ and $v^{\rm rated}$, are set as 314rad/s and 380V, respectively. Meanwhile, as seen in Fig. 4, we set $\rm DG_{1,1}$, $\rm DG_{2,2}$, $\rm DG_{3,1}$, and $\rm DG_{4,1}$ as the pinned DGs from four MGs, respectively, and the adjacency matrices of the lower cyber network can be written as $A_1=A_3=[0,1;1,0]$, $A_2=A_4=[0,1,1;1,0,1;1,1,0]$, and the pinned DG adjacency matrices are $B_1=B_3=\text{diag}\{1,0\}$, $B_2=\text{diag}\{0,1,0\}$, and $B_4=\text{diag}\{1,0,0\}$. While those of the upper cyber network can be written as $\tilde{A}=A_1$, $\tilde{A}=A_2$, and $\tilde{A}=[0,1,0,1;1,0,1,0;0,1,0,1;1,0,1,0]$ respectively for the MG clusters consisting of two MGs(i.e., $\rm MG_1$ and $\rm MG_2$), three MGs(i.e., $\rm MG_1$, $\rm MG_2$, and $\rm MG_3$), and four MGs. Let the sampling period of the DSC scheme for the lower layer $\tau_{\rm sa}=0.0001$s, and the associated input update number $\tau^*=100$. By Algorithm 1(set $\varepsilon=0.02$ and $\tau^*=100$, the

This article has been accepted for publication in a future issue of this journal, but has not been fully edited. Content may change prior to final publication. Citation information: DOI 10.1109/TII.2017.2783334, IEEE Transactions on Industrial Informatics

TABLE I
PARAMETERS FOR THE TEST AC MG CLUSTER SYSTEM

$DG_{1,1}$ & $DG_{2,1}$ & $DG_{2,3}$ & $DG_{3,1}$& $DG_{4,2}$ (71 kVA rating)		$DG_{1,2}$ & $DG_{2,2}$ & $DG_{3,2}$ & $DG_{4,1}$& $DG_{4,3}$ (103 kVA rating)	
V_{DC}	$800V$	V_{DC}	$800V$
K^P	1.6×10^{-5}	K^P	0.8×10^{-5}
K^Q	3×10^{-4}	K^Q	6×10^{-4}
$Load_{1,1}$ & $Load_{1,2}$	$Load_{2,1}$ & $Load_{2,2}$	$Load_{3,1}$ & $Load_{4,1}$	$Load_{3,2}$ &$Load_{4,2}$
$27.5\ kW$ $27.5\ kVar$	$27.5\ kW$ $27.5\ kVar$	$39\ kW$ $39\ kVar$	$29\ kW$ $29\ kVar$
$Line_1$	$Line_{2,1}$	$Line_{2,2}$	$Line_3$
0.64Ω $1.32\ mH$	0.51Ω $1.05\ mH$	0.51Ω $1.05\ mH$	0.58Ω $1.21\ mH$
$TieLine_{12}$	$TieLine_{23}$	$TieLine_{34}$	$TieLine_{41}$
1.73Ω $3.58\ mH$	1.73Ω $3.58\ mH$	1.14Ω $2.38\ mH$	1.14Ω $2.38\ mH$

total iterative number is 3 and elapsed time is 0.001698s.), we obtain the desired learning matrices $\Gamma_s = 0.0004A_s$ and $\Xi_s = 0.0004B_s$ for $s = 1, 2, 3, 4$, $\tilde{\Gamma} = 0.0004\tilde{A}$, the sampling period of the DTC scheme for the upper layer $T_{\rm sa} = 0.01$s, and the associated input update number $T^* = 1$. Thus, inequalities (25) and (26) are satisfied.

During the simulation process, taking the 2-MG cluster test (i.e., MG_1 and MG_2 in Fig. 4) as an example, we implement the two-layer communication network by S-function, S_1, S_2, and $\tilde{S}$, respectively corresponding to the lower communication networks $\mathcal{G}_1$ and $\mathcal{G}_2$, and the upper communication network $\tilde{\mathcal{G}}$. Set sampling periods $\tau^1_{\rm sa} = \tau^2_{\rm sa} = 0.0001$s and $T_{\rm sa} = 0.01$s, and the related input update numbers $\tau^*_1 = \tau^*_2 = 100$ and $T^* = 1$. Then the information interaction within the lower networks $\mathcal{G}_1$ and $\mathcal{G}_2$ will occur every 0.0001s while that within the upper network $\tilde{\mathcal{G}}$ will then occur every 0.01s. However, the control input updates of the lower networks $\mathcal{G}_1$ and $\mathcal{G}_2$ only occur after 100 times information exchange, while that of the upper network $\tilde{\mathcal{G}}$ occurs after each information exchange. By this way, both of the two-layer communication systems have the same terminal time 0.1s so as to drive the two-tier system to output information at the same time.

The next simulation studies cover two scenarios: 1) load change performance assessment (with communication delays, data drop-out, and link failure test), and 2) plug and play capability of MG level (in case of different communication network topologies).

A. Load Change Performance Assessment

This subsection studies the performance of the MG cluster consisting of MG_1 and MG_2 in the situation of load change.

1) General performance assessment: The two MGs are set to be electrically disconnected from each other at $t = 0$s and connected at $t = 2.5$s. Then the tertiary and pinning links, consequently, are disabled at $t = 0$s and activated at $t = 2.5$s correspondingly. After $t = 4$s, the DTC controllers are activated, while $Load_{1,2}$ and $Load_{2,1}$ are removed at $t = 8$s, and then readded at $t = 12$s. Moreover, all DGs consider 314rad/s and 380V as their references when $t \in [0, 2.5)$s. The associated results are given in Figs. 5-7.

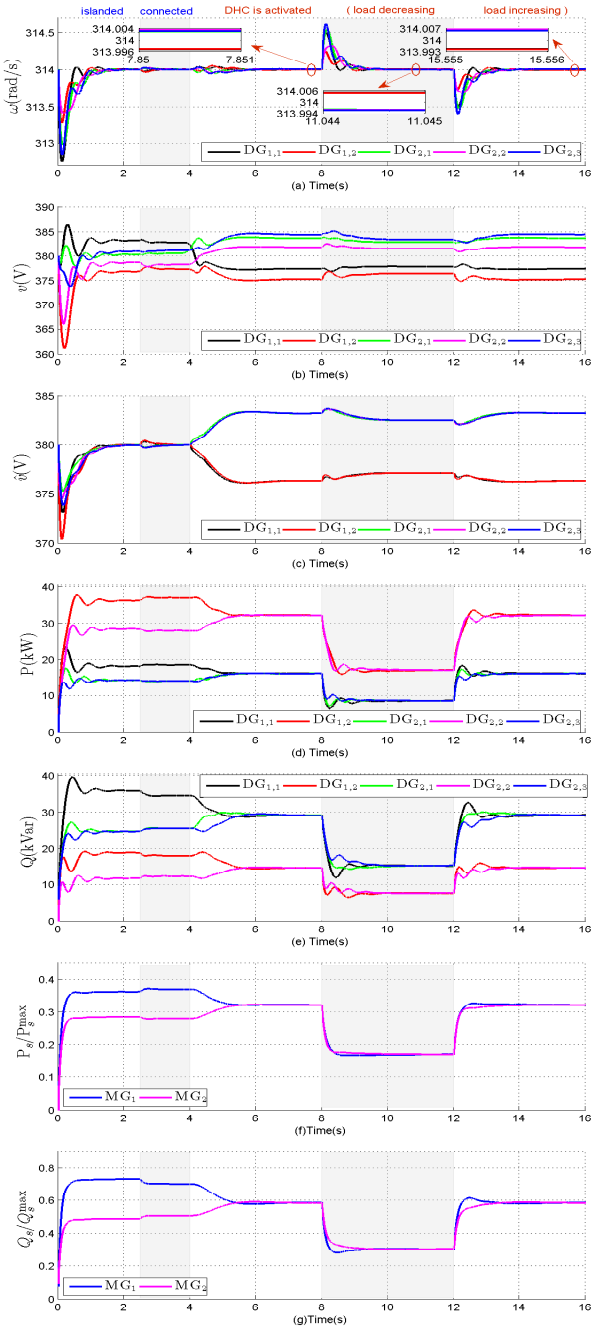

Fig. 5. Performance of the test two MG cluster in case of load change. (a)-(b) frequency/voltage response. (c) voltage estimation. (d)-(e) active/reactive power outputs. (f)-(g) active/reactive output ratios.

As seen in Fig. 5(d)-(e), the DSC scheme proportionally shares the load within each MG before $t = 2.5$s, however, the power outputs among all MGs are different from each other due to the different total local loads. After the DTC scheme is activated at $t = 4$s, the power sharing among MGs is achieved within 4s. After $t = 8$s, the power outputs of each DG vary with the change of local loads within each MG, however, the power sharing among MGs is always maintained, as shown in Fig. 5(f)-(g). Although there exists a little fluctuation for the frequency and voltage response, the excellent steady evolutions can still be observed in Fig. 5(a)-(b). Moreover, due to the inherent contradiction of precise voltage regulation

This article has been accepted for publication in a future issue of this journal, but has not been fully edited. Content may change prior to final publication. Citation information: DOI 10.1109/TII.2017.2783334, IEEE Transactions on Industrial Informatics

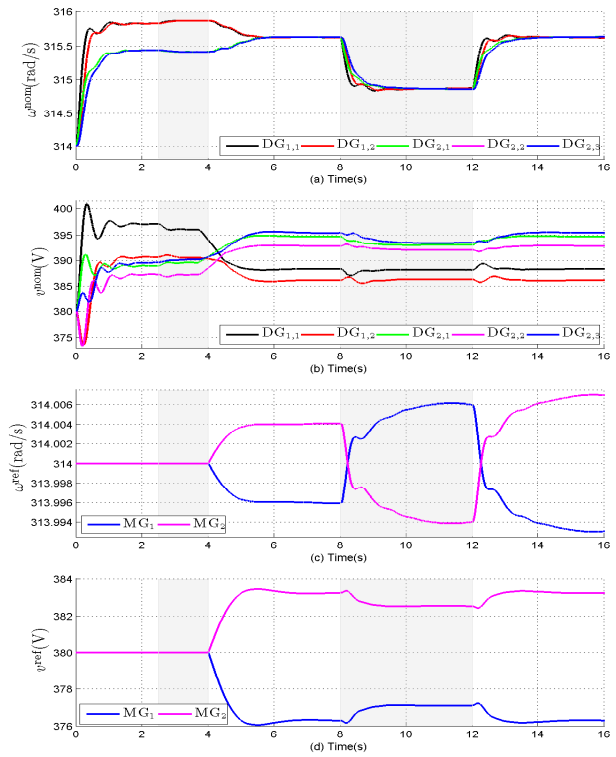

Fig. 6. Reference trajectories of two control layers. (a)-(b) frequency/voltage nominal set-points for primary layer. (c)-(d) frequency/voltage references for secondary layer.

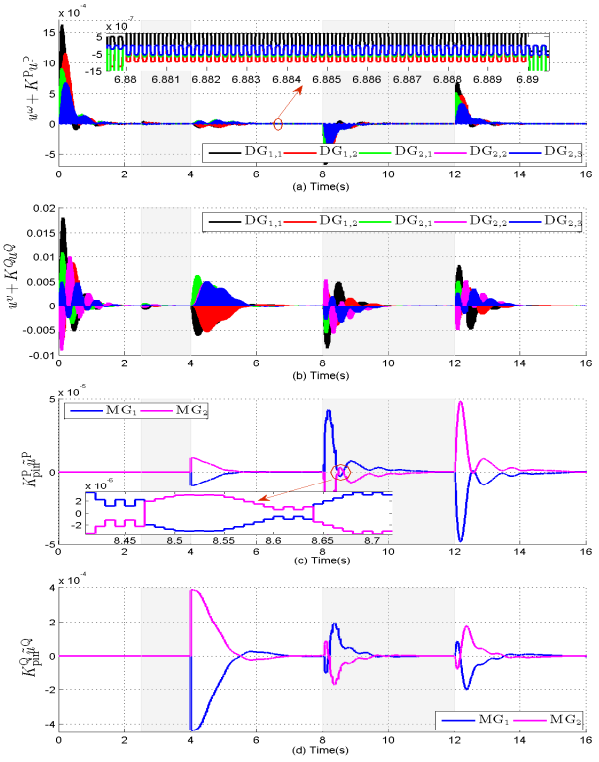

Fig. 7. Control inputs of the reference trajectories. (a)-(b) for primary layer. (c)-(d) for secondary layer.

and reactive power sharing, the designed DSC scheme enables the weighted average voltage of all DGs within MG_s (i.e., the voltage estimation $\hat{v}$) to converge to v_s^{ref} as well as maintains the accurate reactive power sharing (see Figs. 5(c)-6(d)).

Figs. 6-7 show the frequency/voltage references and their control inputs for different control layers, respectively. As seen in Fig. 6(c)-(d), the tertiary references, ω^{ref} and v^{ref}, are designed based on the power output imbalance among MGs, which are then sent to the secondary control layer. While the secondary references, ω^{nom} and v^{nom} as shown in Fig. 6(a)-(b), are obtained by absorbing the state errors among all DGs within each MG. As seen in Fig. 7, the sampling periods and the control input update numbers for different layers are designed differently so as to make a scale separation between the DSC scheme and DTC scheme. In Fig. 8, the selected T^* and T_{sa} do not satisfy (25) and (26). Thus the evolutions of frequency/voltage references and power output curves are fluctuate (see Fig. 8(a)-(d)).

2) Communication delays, data drop-out, and link failure test: The two MGs are set to be electrically disconnected from each other at $t = 0$s and connected at $t = 4$s. Then the tertiary and pinning links, consequently, are disabled at $t = 0$s and activated at $t = 7$s correspondingly. After $t = 7$s, the DTC controllers are activated, while $\mathrm{Load}_{1,2}$ and $\mathrm{Load}_{2,1}$ are removed at $t = 14$s, and then readded at $t = 12$s. Moreover, all DGs consider 314rad/s and 380V as their references when $t \in [0, 4)$s. The three situations are respectively set as: (i) the variable communication delays $d_1(t) = [1.2 + 0.1\sin(t)]/15$ for the lower network and $d_2(t) = [1.5+0.2\sin(t)]/12$ for the upper network. (ii) the data drop-out (packet loss in all links)

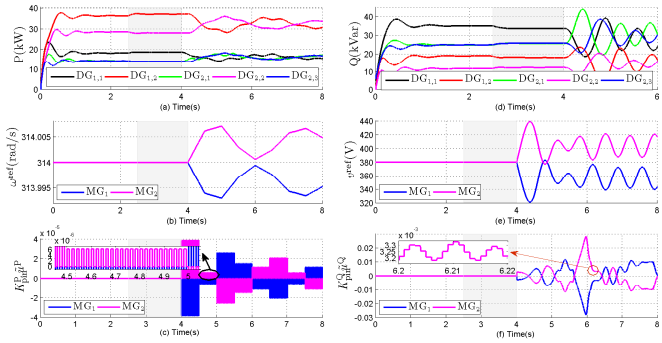

Fig. 8. Performance of the DHC strategy with parameters that do not satisfy (25) and (26). (a)-(c) active power outputs, frequency reference, and control inputs with $T_{\mathrm{sa}} = 0.01$s and $T^* = 50$. (d)-(f) reactive power outputs, voltage reference, and control inputs with $T_{\mathrm{sa}} = 0.001$s and $T^* = 1$.

occurs once in every 15ms, considering 5.5ms communication delays. (iii) the links within MG_1 and MG_2 (i.e., the lower network) are randomly disconnected as $t \in [8, 11]$s and $t \in [15, 18]$s, while the links between MG_1 and MG_2 (i.e., the upper network) are randomly disconnected as $t \in [8, 9.5]$s and $t \in [15, 16.5]$s. The results are given in Figs. 9-10.

As seen, compared with Fig. 5(a),5(b),5(d),and5(e), the convergence time of the system with both DSC and DTC schemes is prolonged by the influence of communication delays (shown in Figs.9(a1),9(a2),10(a1),and10(a2)), data drop-out(shown in Figs.9(b1),9(b2),10(b1),and10(b2)), and link failure (shown in Figs.9(c1),9(c2),10(c1),and10(c2)). Despite this, as verified in Figs. 9-10, the proposed schemes have an acceptable robust performance to these unexpected factors. In detail, for the two-layer communication network with different variable delays

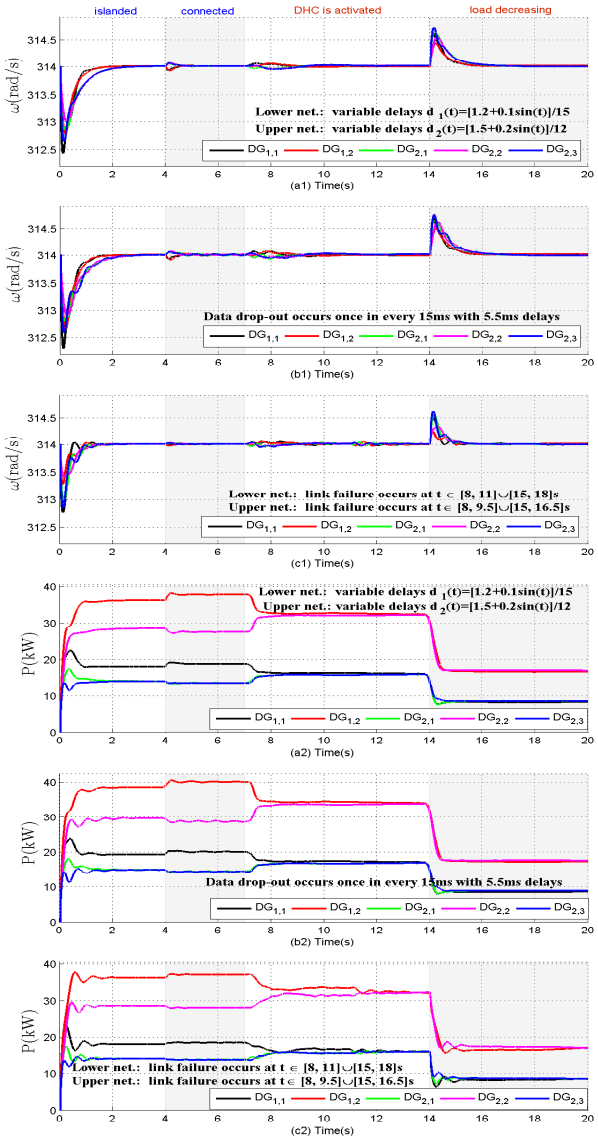

Fig. 9. Frequency response and active power outputs in case of load change with (a1)-(a2) variable communication delays, (b1)-(b2) data-drop out, and (c1)-(c2) link failure.

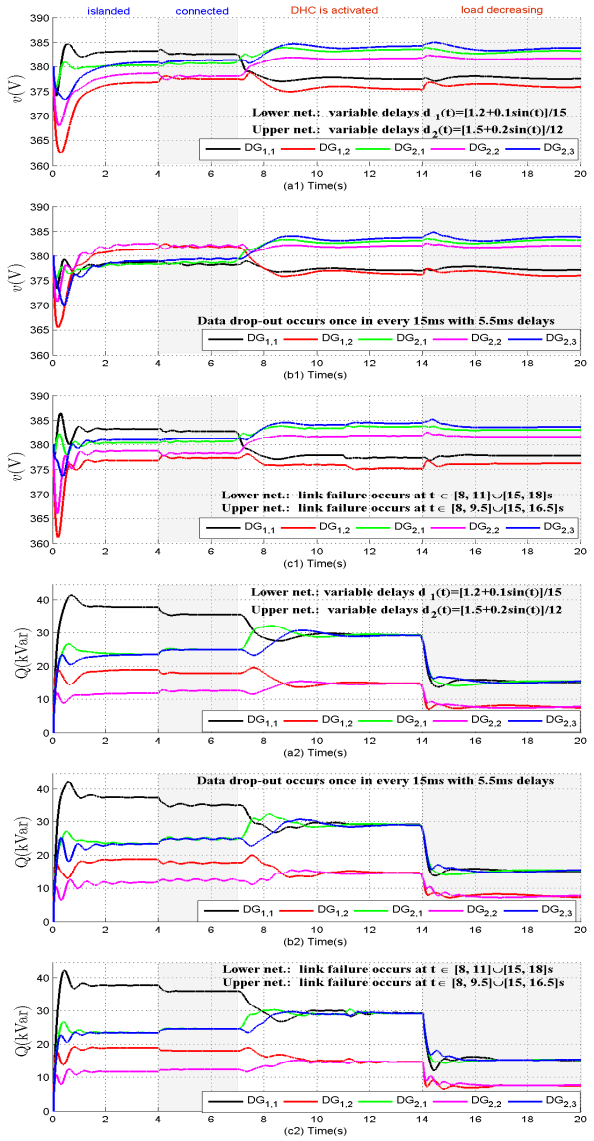

Fig. 10. Voltage response and reactive power outputs in case of load change with (a1)-(a2) variable communication delays, (b1)-(b2) data-drop out, and (c1)-(c2) link failure.

corresponding to different layers, the control performance is still realized in Fig. 9(a1,a2) and 10(a1,a2). Moreover, Comparing these three cases shown in Figs. 9(a2-c2) and 10(a2-c2), we conclude that packet loss will have the worst impact on system stability as $t \in [0, 7]s$. Nevertheless, this kind of unstable evolution curves shown in Figs. 9(b2) and 10(b2) has been stabilized after the DTC scheme is activated at $t = 7$s. Comparing the active/reactive power outputs shown in Fig. 9(c2) and 10(c2) and that shown in Fig. 5(d) and 5(e), it also can be seen that the proposed DTC scheme can suppress the power output instability (during $t \in [8, 11] \cup [15, 18]$s) caused by link failure.

B. Plug and Play Capability of MG Level

This subsection studies the performance of the MG cluster consisting of three MGs and four MGs in the situation of MG plug and play.

1) MG cluster consisting of MG_1, MG_2, and MG_3: All MGs begin to operate separately at $t = 0$s, MG_1 and MG_2 are connected at $t = 2.5$s, while MG_3 is connected and removed respectively at $t = 8$s and $t = 15$s, and the DHC strategy is activated at $t = 4$s. The results are shown in Fig. 11.

As seen, MG_3 is operating in islanded mode before $t = 8$s. When it is connected at $t = 8$s, the frequency/voltage response of each DG begin to vary with the change of the references for each MG (see Fig. 9(a)-(e)), and the power outputs for each MG are redistributed proportionally (see Fig. 11(f)-(g)) within 7s. When MG_3 is removed at $t = 15$s due to some malfunction, its local $\mathrm{Load}_{3,1}$ is also no longer afforded, however, the remaining $\mathrm{Load}_{3,2}$ still needs to afford by the rest MG_1 and MG_2. As seen, the power outputs of MG_3 decline to zero rapidly after $t = 15$s, and the power sharing between the two remaining MGs can still be achieved within 9s.

2) MG cluster consisting of MG_1, MG_2, MG_3, and MG_4: All MGs begin to operate separately at $t = 0$s, MG_1, MG_2,

This article has been accepted for publication in a future issue of this journal, but has not been fully edited. Content may change prior to final publication. Citation information: DOI 10.1109/TII.2017.2783334, IEEE Transactions on Industrial Informatics

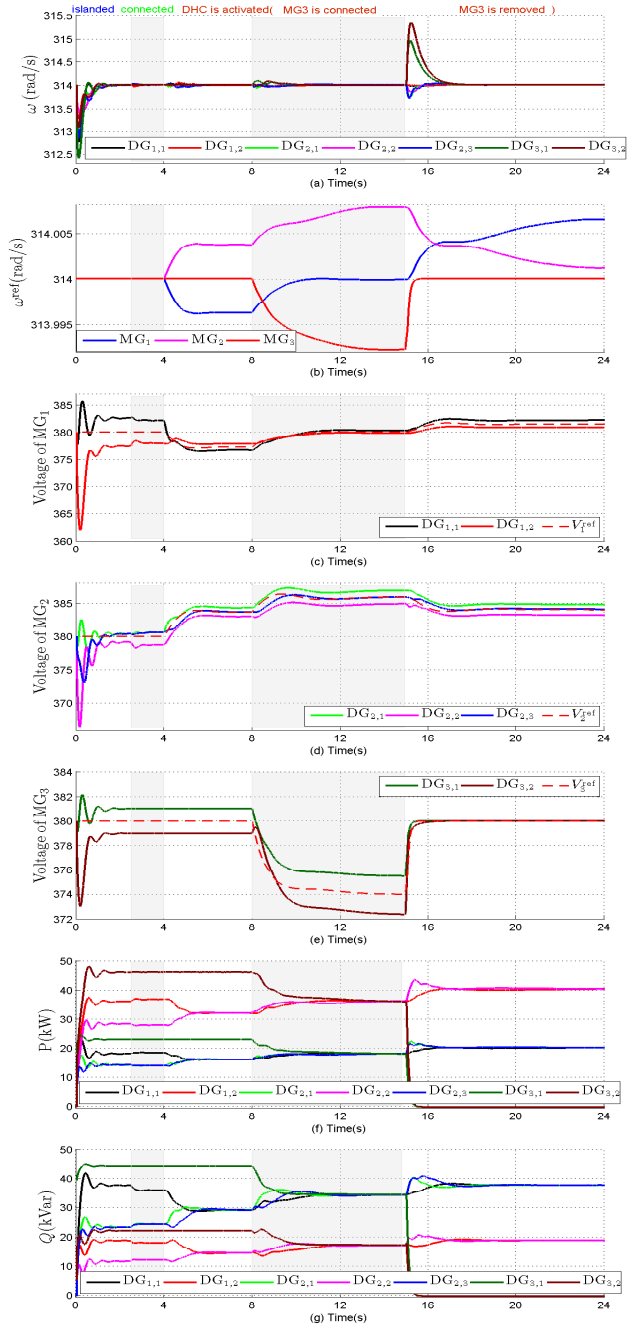

Fig. 11. Performance of the test three MG cluster in case of MG plug and play. (a)-(b) frequency and its reference for the secondary layer. (c)-(e) voltage response for MG_1, MG_2, and MG_3. (f)-(g) active/reactive power outputs.

and MG_4 are connected at $t = 3$s, while MG_3 is connected and removed respectively at $t = 10$s and $t = 18$s, and the DHC strategy is activated at $t = 5$s. To further illustrate the effectiveness of the proposed two-layer network, we implement the proposed scheme on a MG cluster consisting of four MGs under a two-layer digraph (see Fig. 12(a)) and a single-layer digraph (see Fig. 12(b)), and the associated evolution curves are respectively shown in Figs. 13 and 14.

It can be seen by comparing Figs. 13 and 11 that, as the number of the MG increases, the convergence time for the MG cluster consisting of four MGs is longer than that for the case of three MGs. However, the final stability can still be realized.

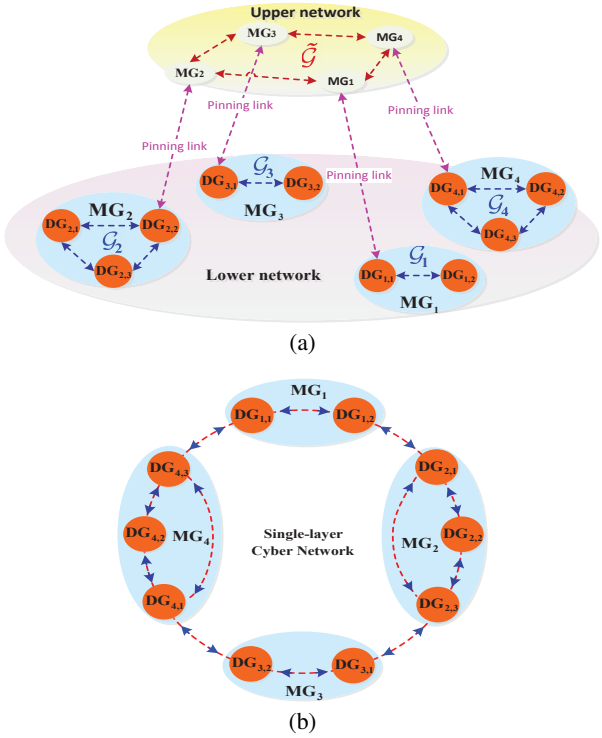

Fig. 12. The test different cyber networks. (a) two-layer network topology: $\tilde{\mathcal{G}}$ and $\{\mathcal{G}\}_{i=1,2,3,4}$ are respectively corresponding to the tertiary and secondary communication, DGs from different MGs have no information interaction during the secondary communication and only the pinned DGs from different MGs participate in the tertiary communication. (b) single-layer network topology: each DG within the same or different MGs is enable to communicate with each other in both the secondary and tertiary communication.

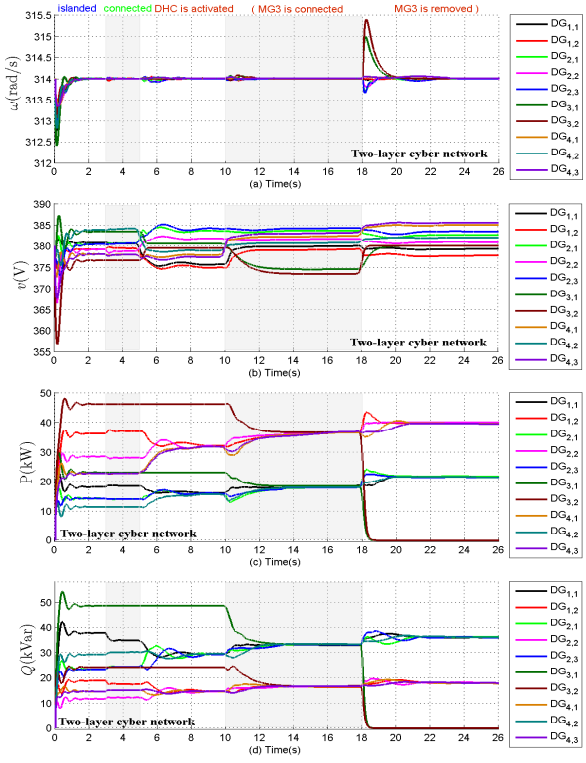

Fig. 13. Performance of the test four MG cluster under two-layer network. (a)-(b) frequency/voltage response. (c)-(d) active/reactive power outputs.

This article has been accepted for publication in a future issue of this journal, but has not been fully edited. Content may change prior to final publication. Citation information: DOI 10.1109/TII.2017.2783334, IEEE Transactions on Industrial Informatics

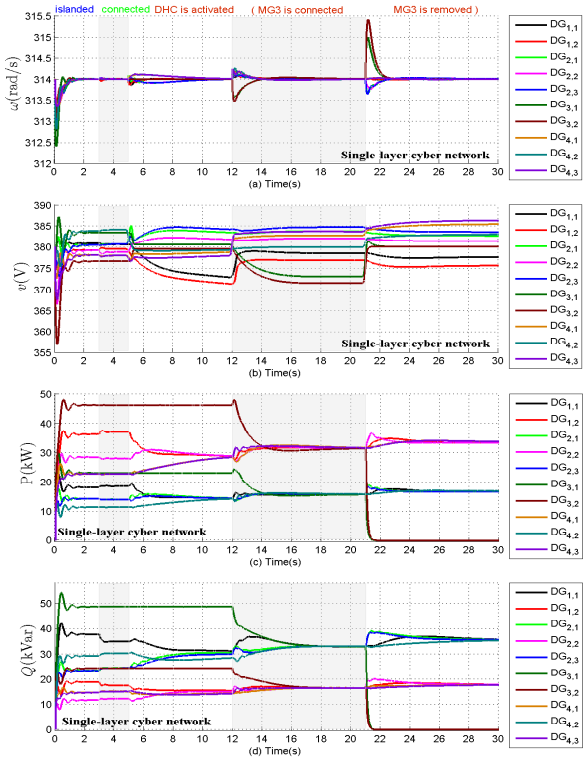

Fig. 14. Performance of the test four MG cluster under single-layer network. (a)-(b) frequency/voltage response. (c)-(d) active/reactive power outputs.

Further, for the proposed DSC and DTC schemes implemented in a single-layer digraph (Fig. 12(b)), it can be found that the corresponding performance is a little worse than the case of two-layer digraph (Fig. 12(a)) by comparing the evolution curves shown Figs.13 and 14. In fact, the DSC and DTC schemes are designed to implement in different dynamics with different time scales, while a two-layer digraph can effectively meet the time-scale separation requirements for the interactive information flow that integrated in the cluster-oriented physical network. Moreover, each DG within each MG has the same control property and thus is responsible to implement both the secondary and tertiary communication tasks in the single-layer digraph. But for the two-layer digraph, DGs within different MGs have no information interaction with each other during the secondary communication stage, and only the pinned DGs within each MG participate in the tertiary control decision process and thus possess the tertiary communication task. The associated control costs for the two-layer network are therefore less than that of the single-layer network.

VI. Conclusion

A DHC strategy for islanded AC MG cluster systems is presented, which can regulate the frequency/voltage within each MG as well as maintain the active/reactive power sharing among AC MGs with heterogenous DGs. By pinning one or some DGs from each MG to constitute an upper cyber network, a two-layer sparse cyber network is formulated to support the dynamical coupling between the secondary and tertiary levels. Moreover, the time response matching problem has been studied, which indicates that the stability can be guaranteed if the sampling period ratio of the tertiary to secondary is less than a certain upper bound. All the distributed controllers are equipped with discrete iterative inputs that are merely updated at the end of each round of iteration, which permits an intermittent communication manner. In practical, how to solve the load uncertainty problem based on the designed two-layer network will be our future work.

VII. Appendix

Lemma 1: If the graph $\mathcal{G}_s$ for MG_s is connected, then the designed voltage observer (6) can ensure that

$$\lim_{k\to\infty}\left|\hat{v}_{s,i}(t_k^{\tau^*})-\mu_{s,i}v_{s,i}(t_k^{\tau^*})\right|=0,\ i\in\mathcal{I}_{m_s}, s\in\mathcal{I}_M. \quad (27)$$

Proof: By the previous denotations, rewrite (6) as

$$\hat{v}_s(t_k^{\ell+1})=(I_{m_s}-L_s)\hat{v}_s(t_k^{\ell})+v_s(t_k^{\ell+1})-v_s(t_k^{\ell}). \quad (28)$$

Let $\hat{V}_s(z)$, $V_s(z)$ be the Z-transforms of $\hat{v}_s(t_k^{\ell})$, $v_s(t_k^{\ell})$, then

$$\hat{V}_s(z)=(z-1)[(z-1)I_{m_s}+L_s]^{-1}V_s(z). \quad (29)$$

Since the transfer function $(z-1)[(z-1)I_{m_s}+L_s]^{-1}$ is stable if the first inequality in (25) holds, then consider the discrete dynamic $x(\ell+1)=(I_{m_s}-L_s)x(\ell)$ associated with this transfer function. If $\mathcal{G}_s$ is connected, there exists a positive left eigenvector μ_s corresponding to the zero eigenvalue of L_s such that $\sum_{i=1}^{m_s}\mu_i^s x_i(\ell)$ is an invariant quantity. By the final value theorem, we deduce the desired objective (27). ■

References

[1] X. Yu, and Y. Xue, "Smart grids: a cyber-physical systems perspective", *Proceedings of the IEEE*, vol.104, no.5, pp.1058-1070, May, 2016.

[2] M. Yazdanian, and A. Mehrizi-Sani, "Distributed control techniques in microgrids", *IEEE Trans. Smart Grid*, vol.5, no.6, pp.2091-2099, Oct. 2014.

[3] N. Nikmehr, S.N. Ravadanegh, "Optimal power dispatch of multi-microgrids at future smart distribution grids", *IEEE Trans. Smart Grid*, vol. 6, no.4, pp.1648-1657, Jul. 2015.

[4] B. Robbins, C. Hadjicostis, and A. Dominguez-Garcia, "A two-stage distributed architecture for voltage control in power distribution systems", *IEEE Trans. Power Syst.*, vol. 28, no. 2, pp.1470-1482, May. 2013.

[5] T. Vandoorn, J.De Kooning, and B. Meersman, "Review of primary control strategies for islanded microgrids with power-electronic interfaces", *Renew. Sustain. Energy Rev.*, vol. 19, pp. 613-628, Mar. 2013.

[6] X. Lu, J. M. Guerrero, K. Sun, J. Vasquez, *et. al*, "Hierarchical control of parallel AC-DC converter interfaces for hybrid microgrids", *IEEE Trans. Smart Grid*, vol.5, no.2, pp.683-692, Jul. 2014.

[7] Q.C. Zhong, "Robust droop controller for accurate proportional load sharing among inverters operated in parallel", *IEEE Trans. Ind. Electron.*, vol. 60, no. 4, pp.1281-1290, Apr. 2013.

[8] L. Meng , F. Tang , M. Savaghebi , J.C. Vasquez, J.M. Guerrero, "Tertiary control of voltage unbalance compensation for optimal power quality in islanded microgrids", *IEEE Trans. Energy Conversion.*,vol. 29, no4, pp.802-815, Dec. 2014.

[9] M. Erol-Kantarci, B. Kantarci, and H. T. Mouftah, "Reliable overlay topology design for the smart microgrid network", *IEEE Network*, vol. 25, no.5, pp.38-43, Sep. 2011.

[10] A. Bidram, A. Davoudi, F.L. Lewis, and J. M. Guerrero, "Distributed co-operative secondary control of microgrids using feedback linearization", *IEEE Trans. Power Syst.*, vol.28, no.3, pp.3462-3470, Aug. 2013.

[11] Q. Shafiee, J.M. Guerrero, and J.C. Vasquez, "Distributed secondary control for islanded microgrids–A novel approach", *IEEE Trans. Power Electron.*, vol. 29, no. 2, pp.1018-1031, Feb. 2014.

[12] J.W. Simpson-Porco, Q. Shafiee, F. Dörfler, J.M. Guerrero, and F. Bullo, " Secondary frequency and voltage control of islanded microgrids via distributed averaging", *IEEE Trans. Ind. Electron*, vol. 62, no. 11, pp.7025-7038, Nov. 2015.

[13] J. Lai, H. Zhou, X. Lu, X. Yu, and W.S. Hu, "Droop-based distributed cooperative control for microgrids with time-varying delays", *IEEE Trans. Smart Grid*, vol. 7, no. 4, pp.1175-1189, Jul. 2016.

[14] X. Lu, X. Yu, J. Lai, Y. Wang, and J. M. Guerrero, "A novel distributed secondary coordination control approach for islanded microgrids", *IEEE Trans. Smart Grid*, 2017, to be published, doi: 10.1109/TSG.2016.2618120.

[15] X. Lu, X. Yu, J. Lai, J.M. Guerrero, and H. Zhou,"Distributed secondary voltage and frequency control for islanded microgrids with uncertain communication links", *IEEE Trans. Ind. Infor.*, vol. 13, no. 2, pp.448-460, Apr. 2017.

[16] J.M. Guerrero, M. Chandorkar, T. Lee, and P. Loh, "Advanced control architectures for intelligent microgrids, part I: decentralized and hierarchical control", *IEEE Trans. Ind. Electron*, vol. 60, no.4, pp.1254-1262, Apr. 2013.

[17] L. Meng, T. Dragicevic, J.C. Vasquez, and J.M. Guerrero, "Tertiary and secondary control levels for efficiency optimization and system damping in droop controlled dc-dc converters", *IEEE Trans. Smart Grid*, vol. 6, no. 6, pp. 2615-2626, Nov, 2015.

[18] D. Niyato, P. Wang, "Reliability analysis and redundancy design of smart grid wireless communications system for demand side management", *IEEE Wireless Commun.*, vol. 19, no.3, pp.38-46, June 2012.

[19] L. Wu, J. Li, M. Erol-Kantarci, and B. Kantarci, "An integrated reconfigurable control and self-organizing communication framework for community resilience microgrids", *The Electricity Journal*, vol. 30, no. 4, pp. 27-34, May 2017.

[20] A. Arefi, F. Shahnia, "Tertiary controller-based optimal voltage and frequency management technique for multi-microgrid systems of large remote towns", *IEEE Trans. Smart Grid*, 2017, to be published, doi: 10.1109/TSG.2017.2700054.

[21] Q. Shafiee, T. Dragievi, J.C. Vasquez, and J.M. Guerrero, "Hierarchical control for multiple DC microgrids clusters", *IEEE Trans. Energy Convers.*, vol. 29, no.4, pp.922-933, Oct. 2014.

[22] S. Moayedi, and A. Davoudi, "Distributed tertiary control of dc microgrid clusters", *IEEE Trans. Power Electron.*, vol. 31, no.2, pp.1717-1733, Feb. 2016.

[23] A. Maknouninejad, Z. Qu, J. Enslin, and N. Kutkut, "Clustering and cooperative control of distributed generators for maintaining microgrid unified voltage profile and complex power control", *in Proc. IEEE PES Transm. Distrib. Conf. Expo.*, pp. 1-8, May. 2012.

[24] I.U. Nutkani, P.C. Loh, and F. Blaabjerg, "Distributed operation of interlinked AC microgrids with dynamic active and reactive power tuning", *IEEE Trans. Ind. Appl.*, vol. 49, no.5, pp.2188-2196, Sep. 2013.

[25] S. Weckx, R. D'hulst, and J. Driesen, "Primary and secondary frequency support by a multi-agent demand control system", *IEEE Trans. Power Syst.*, vol. 30, no. 3, pp.1394-1404, May. 2015.

[26] Q.Y. Sun, R.K. Han, H.G. Zhang, J.G. Zhou, and J. M. Guerrero,"Multi-agent-based consensus algorithm for distributed coordinated control of distributed generators in the energy internet", *IEEE Trans. Smart Grid*, vol.6, no.6, pp.3006-3019, Nov. 2015.

[27] T. L. Vandoorn, J. C. Vasquez, J. D. Kooning, J. M. Guerrero, and L. Vandevelde, "Microgrids: hierarchical control and an overview of the control and reserve management strategies", *IEEE Ind. Electron. Mag.*, pp. 42-55, Dec. 2013.

[28] W. Liu, W. Gu, W. Sheng, X. Meng, S. Xue, and M. Chen, "Pinning-based distributed cooperative control for autonomous microgrids under uncertain communication topologies", *IEEE Trans. Power Syst*, vol. 31, no. 2, pp. 1320-1329, Mar. 2016.

[29] X. Lu, Y. Wang, X. Yu, and J. Lai, "Finite-time control for robust tracking consensus in MASs with an uncertain leader," *IEEE Trans. Cybern.*, vol. 47, no.5, pp.1210-1223, May 2017.

[30] R. Horn and C. Jornson. Matrix analysis. New York: Cambridge University Press; 1985.

Xiaoqing Lu received the M.Sc. and Ph.D. degrees in applied mathematics from Wuhan University, Wuhan, China.

She is currently a Professor in the School of Power and Mechanical Engineering, Wuhan University, Wuhan, China. She is also a Postdoctoral Research Fellow at the School of Engineering, RMIT University, Melbourne, Australia. Her research interests include nonlinear dynamical systems, intelligent systems and applications, complex networks, multi-agent systems, and microgrids.

Jingang Lai (M'17) received the M.Sc. degree in control science and engineering from the Wuhan University of Technology, Wuhan, China, in 2013, and Ph.D. degree from Department of Automation, Wuhan University, Wuhan, China, in 2016. He was a Visiting Ph.D. Student in the School of Electrical and Computer Engineering, RMIT University, Melbourne, VIC, Australia, in 2015.

He is currently a Visiting Research Fellow in the School of Engineering, RMIT University, Melbourne, VIC, Australia. His current research interests include smart grid and networked control systems.

Xinghuo Yu (M'92-SM'98-F'08) received the B.Eng. and M.Eng. degrees from the University of Science and Technology of China, Hefei, China, in 1982 and 1984, respectively, and the Ph.D. degree from Southeast University, Nanjing, China, in 1988.

He is currently with RMIT University (Royal Melbourne Institute of Technology), Melbourne, VIC, Australia, where he is Associate Deputy Vice- Chancellor Research Capability and Distinguished Professor. His current research interests include variable structure and nonlinear control, and complex and intelligent systems and applications.

Prof. Yu was a recipient of a number of awards and honors for his contributions, including the 2013 Dr.-Ing. Eugene Mittlemann Achievement Award of the IEEE Industrial Electronics Society and the 2012 *IEEE Industrial Electronics Magazine* Best Paper Award. He is President-Elect (2016-2017) of the IEEE Industrial Electronics Society.

Yaonan Wang (SM'94) received the B.S. degree in computer engineering from East China Science and Technology University (ECSTU), Fuzhou, China, in 1981, and the M.S. and Ph.D. degrees in electrical engineering from Hunan University, Changsha, China, in 1990 and 1994, respectively.

He is currently a Professor with the College of Electrical and Information Engineering, Hunan University. From 1994 to 1995, he was a Post-Doctoral Research Fellow with the National University of Defense Technology, Changsha. From 1981 to 1994, he was with ECSTU. From 1998 to 2000, he was a Senior Humboldt Fellow in Germany, and from 2001 to 2004, he was a Visiting Professor with the University of Bremen, Bremen, Germany. His current research interests include intelligent control, image processing, and intelligent robotics.

Josep M. Guerrero (S'01-M'04-SM'08-F'15) received the B.S. degree in telecommunications engineering, the M.S. degree in electronics engineering, and the Ph.D. degree in power electronics from the Technical University of Catalonia, Barcelona, Spain, in 1997, 2000, and 2003, respectively.

Since 2011, he has been a Full Professor with the Department of Energy Technology, Aalborg University, Aalborg, Denmark, where he is responsible for the Microgrid Research Program. From 2012, he is a Guest Professor at the Chinese Academy of Science, Beijing, China and the Nanjing University of Aeronautics and Astronautics, Nanjing, China; from 2014, he is Chair Professor in Shandong University, Jinan, China; and from 2015, he is a Distinguished Guest Professor in Hunan University, Changsha, China. His research interests include different microgrid aspects, including power electronics, distributed energy-storage systems, hierarchical and cooperative control, energy management systems, and optimization of microgrids and islanded minigrids.